UNIVERSITAT POLITÈCNICA DE CATALUNYA
UPC

UNIVERSITAT DE BARCELONA
UB

Proyecto Final de Estudios

**MÁSTER
EN
INGENIERÍA BIOMÉDICA**

EB

Sample-Specific Computational Fluid Dynamics of Vascular Network Functionality

Barcelona, 7 de Julio del 2011

Autor: Aura María Cardona Ochoa

Director: Damien Lacroix

Realizado en: Instituto de Bioingeniería de Cataluña (IBEC)

UNIVERSITAT POLITÈCNICA DE CATALUNYA

UNIVERSITAT DE BARCELONA

Data de registre: 09/05/11

MÀSTER ENGINYERIA BIOMÈDICA

Registre Projecte Final d'Estudis

NOM DE L'ALUMNE: Aura Maria Cardona Ochoa

TÍTOL DEL PROJECTE: Sample-specific computational fluid dynamics of vascular network functionality.

DIRECTOR/S DEL PROJECTE:
(Indiqueu Centre, Departament,
Empresa, Hospital, etc. on està vinculat el director)

Damien Lacroix, PhD, Biomechanics & Mechanobiology, Institute for Bioengineering of Catalonia
C\ Baldiri Reixac, 4 08028 Barcelona-Spain
Tel: +34 934020266
Email: dlacroix@ibecbarcelona.eu
http://www.biomechanics.es

DNI . Y0996540T
NIUB : 15308425.

Dr.
Director del projecte

Signatura de l'alumne

Dr. Pere Caminal
Coordinador UPC
Màster Enginyeria Biomèdica
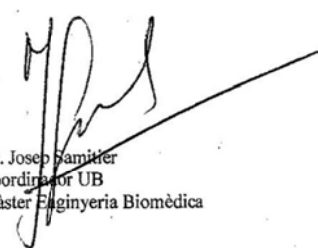
Dr. Josep Samitier
Coordinador UB
Màster Enginyeria Biomèdica

Economic support

Master Subjects

- Biomaterials
- Biomedical Imaging
- Methods for Modeling and Simulating Biosystems
- Tissue Engineering
- Biomedical Signals (recognized credits)
- Biomedical Devices (recognized credits)
- Clinical Engineering and Healthcare Models (recognized credits)

Presentations resulting from this Study

Second TOPEA Summer School, Imaging in tissue regeneration, June 30 and July 1 Barcelona 2011, Parc de Recerca Biomèdica de Barcelona (PRBB).

Acknowledgements

I am glad to express my gratitude to those who have contributed to the research performed and writing of this Master thesis.

First of all, I gratefully acknowledge the invaluable collaboration of my director and supervisor Damien Lacroix, from the group of Biomechanics and Mechanobiology of the Institute for Bioengineering of Catalonia (IBEC), who has guided me during the whole year to achieve and well focus my project. It is a fortune to have him as a supervisor.

Furthermore, I would like to thank the economic support to this study provided by the European Commission (Angioscaff FP7) and the Institute for Bioengineering of Catalonia (IBEC). A special thanks to Laura Nebuloni from the Swiss federal Institute of Technology Zurich (ETHZ) for always taking the time to help me, for her patience and cooperation.

Finally, I thankfully appreciate the several contributions provided by different people in the group of Biomechanics and Mechanobiology such as Clara Sandino, Sara Barreto, Andy Olivares, Andrea Malandrino, Jérôme Noailly and Cécile Perrault, and also to Diego Reginensi and Adrià Muñoz. Thanks to their contributions have made possible the successful development of this project.

Contents

List of Figures

7

List of Tables

Abbreviations

3D	Three – Dimensional
2D	Two - Dimensional
μCT	Micro-Computed Tomography
CAD	Computer-Aided Design
CPU	Central Processing Unit
CFD	Computational Fluid Dynamics
CT	Computer Tomography
DC	Dicom
ECM	Extracellular Matrix
ECs	Endothelial Cells
ETHZ	Swiss Federal Institute of Technology Zurich
FE	Finite Elements
FEA	Finite Element Analysis
FEM	Finite Element Method
MRI	Magnetic Resonance Imaging
NDE	Nondestructive Evaluation
PDE	Partial Differential Equation
RAM	Random-Access Memory
RX	X-rays
STL	Stereolithography
SR	Synchrotron Radiation
TE	Tissue Engineering
VEGF	Vascular Endothelial Growth Factor
VOI	Volume of Interest
WSS	Wall Shear Stress

Abstract

One of the main factors to control in the development of tissue engineering scaffolds is the growth of new blood vessels and the posterior formation of vascular networks, which is consider as a critical factor because of the transport of nutrients and oxygen to the surrounding cells.

Nowadays, computational modeling is presented as a useful support tool to provide a better understanding of vascular networks functionality. Therefore, the analysis of large-scale computational fluid flow dynamics (CFD), allows us to obtain the local parameters associated to mechanical stimuli affecting the microenvironment (scaffolds) and tissue involved (vascular cells). This study has developed a robust methodology to perform a quantitative assessment of vascular networks functionality based on numerical simulations.

The methodology to perform the CFD analyses presented in this study is based on two different samples. The vascular networks were obtained by Synchrotron and Micro-Computed Tomography provided by the Swiss Federal Institute of Technology Zurich in DICOM file format.

The DICOM files were imported in Simpleware to obtain a three dimensional reconstruction, superficial and solid mesh of the vascular networks. Due to the complexity of the structure and the amount of data generated, an optimization scheme was defined to reduce computing time while maintaining the accuracy of the results.

Once the mesh was obtained, the boundary conditions and the properties of the fluid were defined in Fluent and Tdyn to simulate blood movement from the superior to inferior position. The results allowed us to interpret the mechanical phenomenon involved in the angiogenesis process and the importance of cellular responses to mechanical stimuli in tissue engineering applications.

Resumen

Uno de los principales factores a controlar en el desarrollo de andamios en ingeniería de tejidos, es el crecimiento de nuevos vasos sanguíneos y la posterior formación de redes vasculares dentro de los mismos. El desarrollo de estos vasos es necesario principalmente, para transportar nutrientes y oxígeno a las células circundantes y mantener la viabilidad de estas células al interior de los andamios.

Hoy en día, el modelado computacional se presenta como una herramienta útil en el campo de la hemodinámica, capaz de proporcionar una mejor comprensión de la funcionalidad de las redes vasculares en diferentes campos de la medicina y de la bioingeniería. El análisis de la dinámica de fluidos computacional (CFD) a gran escala, nos permite la obtención de los parámetros locales asociados a los estímulos mecánicos que afectan el microambiente (andamios) y el tejido circundante (células vasculares) de las redes vasculares. En este estudio se ha desarrollado una metodología robusta para llevar a cabo una evaluación cuantitativa de la funcionalidad de redes vasculares basada en simulaciones numéricas.

La metodología para llevar a cabo el análisis CFD presentada en este estudio está basada en dos muestras diferentes de redes vasculares obtenidas mediante Sincrotrón y Micro-Computer Tomography (µCT), proporcionadas por el Swiss Federal Institute of Technology Zurich (ETHZ) en formato DICOM (DC).

Los ficheros DC fueron importados en Simpleware para obtener la reconstrucción tridimensional de las redes vasculares, y la construcción de mallas superficiales y sólidas de las mismas. Debido a la complejidad de la estructura y a la cantidad de datos generados, se definió un esquema de optimización para reducir el tiempo de cómputo y calculo mientras que se mantuvo la precisión de los resultados.
Una vez la malla fue obtenida, las condiciones de frontera y las propiedades del fluido fueron definidas en Fluent y Tdyn para simular el movimiento de la sangre desde la posición superior a la inferior de la red. Los resultados nos llevan a interpretar el fenómeno mecánico involucrado en el proceso de angiogénesis en las aplicaciones de ingeniería de tejidos y la importancia de las respuestas celulares a los diferentes estímulos mecánicos.

Chapter 1 Angiogenesis in Tissue Engineering: State of the Art

1.1 Introduction

Biomaterials that promote angiogenesis have great potential in regenerative medicine for rapid revascularization of damaged tissue, survival of transplanted cells, and healing of chronic wounds. Ghannaati et al. have designed biomaterials to promote angiogenesis from supra-molecular nanofibers formed by self-assembly to evaluate the vascularization within these biomaterials [1].

However, the techniques used normally are not enough to induce the rapid vascularization necessary for an adequate cellular oxygen supply. Thus, nowadays researchers focus on the creation of μ-vascular networks within 3D tissue constructs *in vitro* before implantation using *in vivo* models (chicken embryo and dorsal skinfold chamber) [2].

After obtaining the vascularization within the scaffolds it is necessary to quantify this vasculature. Some approximations have been made to quantify the total volume of the capillary network within the scaffolds [3] characterizing μ-vessel within scaffolds in physiological *in vivo* tissue engineering implant context.

However, qualitative studies of growth and performance of these μ-capillaries within the scaffolds to report velocity, pressure and wall shear stress (WSS) profiles to determine and analyze their functionality have not been done yet.

So far, there are only functional analysis of large vessels and simple networks and there are not enough reports from μ-vessels and big networks. Lee et al. [4] have done a 3D computational flow modeling of a wide angle bifurcation and they have analyzed WSS, blood velocity, and blood pressure profiles in a chicken embryo model.

Nowadays, measure of WSS, velocity or pressure within tissue constructs to evaluate the functionality of μ-vascular networks *in vitro* or *in vivo* is difficult and expensive. Gödde and Kurz [5] modeled blood flow through capillary networks to determine local pressure gradients, which were in turn used to calculate local shear stress. Also blood flow, pressures and shear stresses on ECs have been proposed and modeled as angiogenic stimuli [5,6].

Therefore, to perform a quantitative assessment of the functionality of the μ-vascular network based on the numerical simulations turns out to be a useful support tool for predicting the functionality of this new vascular network within the scaffolds design in the Angioscaff Project and then to be compared with results obtained *in vitro* and *in vivo* from the same project.

1.2   The Principles Neo-vascular System: Structure and Function of Vascular System

The term angiogenesis is reserved to describe the formation of new vessels, usually at the capillary level, by proliferation, migration, and assembly of endothelial cells from existing capillaries or venules [7]. This new microvasculature is an extremely adaptable structure that is capable of architectural and functional adjustments in response to multiple biochemical and mechanical stimuli [8].

The fundamental function of the vascular system is to deliver oxygen and nutrients to the cells and remove waste from peripheral tissues.

There are three main types of blood vessels: arteries, veins, and capillaries. All blood vessels except capillaries have three distinct layers surrounding a central blood carrying lumen (**Figure 1**) [9].

d = Lumen Diameter

h = Wall Thickness

Name of Vessel	Aorta	Artery	Arteriole	Capillary	Venule	Vein	Vena Cava
Number of Vessel	1	100*	10^8*	10^{10}*	10^9*	100*	2
Lumen Diameter (mm)	25	4	0.03	0.008	0.02	5	30
Wall Thickness (mm)	2	1	0.02	0.001	0.002	0.5	1.5
Wall Composition Endothelium Elastic Tissue Smooth Muscle Fibrous Tissue							
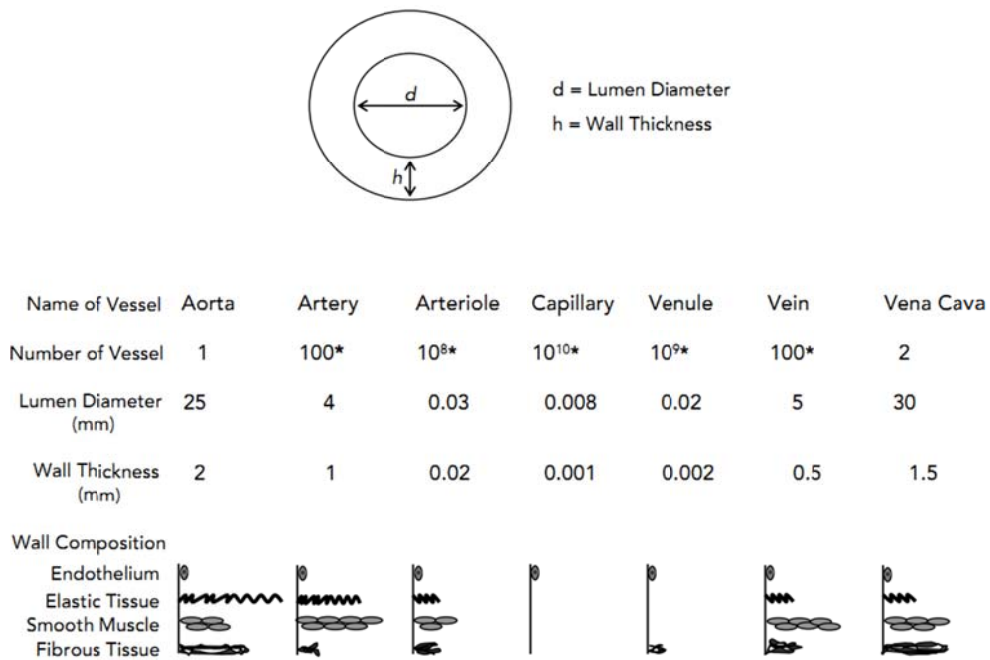
Figure 1 Comparison between different types of blood vessels. *: Approximate numbers [9]

Microcirculation refers to the flow of blood between arterioles and venules through capillaries (Figure 2) .The capillaries arising from a single arteriole typically form an interconnecting network, called a capillary bed, to serve a discrete area of tissue [8].
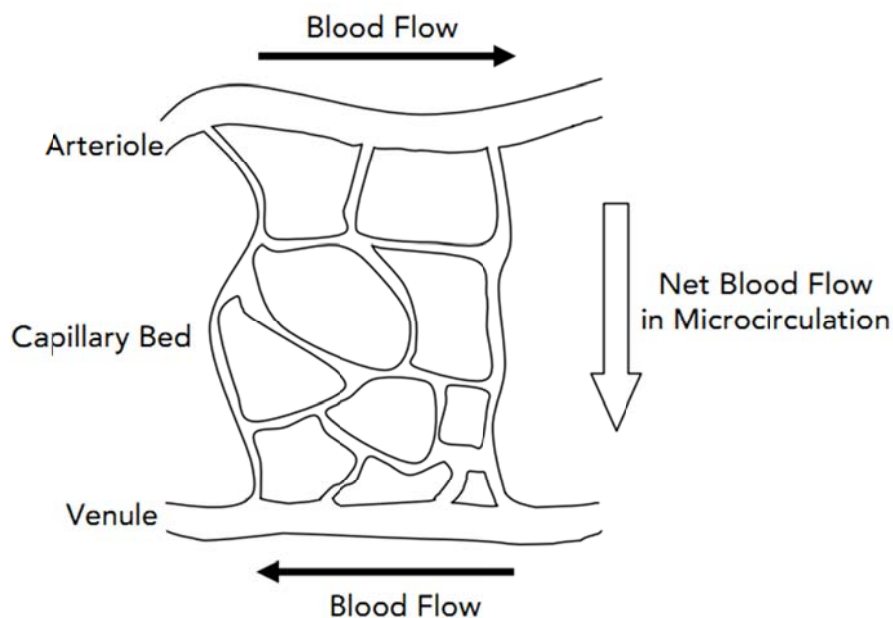
Figure 2 Microcirculation and interendothelial junctions [9]

1.3   Angiogenesis

During the process of angiogenesis are distinguished vasculogenesis that occurs to establish the vascular pattern of the adult and the formation of new capillaries. It occurs infrequently in healthy adults, except during ovulation, pregnancy, wound healing, and exercise training [10]. The fundamental role of angiogenesis in a large number of different and unrelated diseases and in several bioengineering applications has become this process in a focus of attention for many scientists from various fields [11]. In the field of bioengineering, the performance of the angiogenesis process in tissue engineering is limited by an inadequate transport between the tissue and the blood vessels [12].

Promoting vascular growth toward or within these tissue constructs is a key element to their success. Thus, there has been extensive effort made to develop strategies for controlling pathological angiogenesis and for promoting vascularization in biomedical engineering applications [9].

Angiogenesis is regulated by several micro-environmental factors in the blood vessels, including soluble molecules (e.g., growth factors and cytokines), extracellular matrices (ECM), interactions between adjacent endothelial cells (ECs) and ECs with other cell types, as well as mechanical forces originating from ECs themselves, blood flow, and extravascular tissue activity (**Figure 3**) [13].
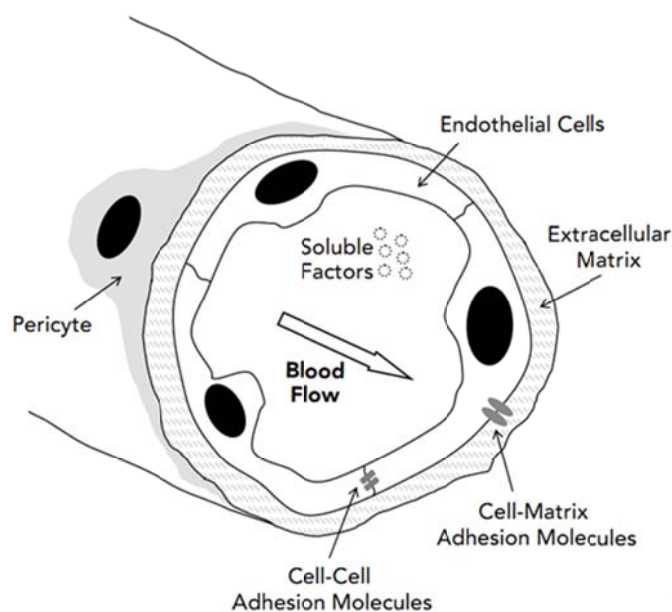
Figure 3 Microenvironmental factors that can affect angiogenesis [9]

1.4   Biomechanics of Angiogenesis

All cells in the body, including ECs, are subjected to mechanical forces that either are self-generated or originate from the environment during common physiological processes.

In contrast to the wealth of information about the biochemical aspect of angiogenesis regulation, knowledge of the contribution of mechanical forces and mechanical stimulus in the angiogenesis process is very limited [9].

Blood vessels are constantly exposed to mechanical forces that originate from blood flow or the extravascular environment (**Figure 4**). There is a vast amount of experimental evidence demonstrating that externally applied mechanical stresses (fluid shear stress, stretch, and pressure) regulate cytoskeletal organization, signal transduction, gene expression, and a wide variety of ECs functions, including migration, proliferation, and ECM remodeling, which suggests a role of extrinsic stresses in angiogenesis.
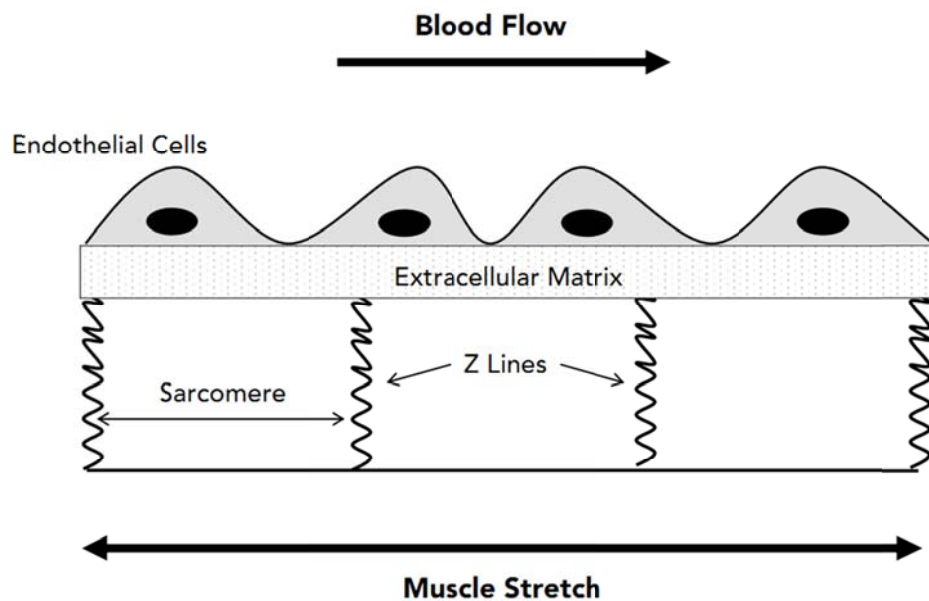
Figure 4 Externally applied mechanical stresses on endothelial cells [9]

In fact, many studies have shown that fluid shear stress and stretch can affect the production or activity of the endogenous biochemical factors [9]. There are several reviews concerning the effects of externally applied mechanical stimulus on ECs functions [14].

The role of blood flow in capillary growth was first demonstrated by Clark in the late 1910s [15] by examining capillaries in the same area in tad-pole tails for many consecutive days, Clark was able to prove that capillaries with a high velocity of flow (and with a high shear stress) had more sprouts, but capillaries with slow flow gradually narrowed and disappeared.

1.5   Tissue Engineering

1.5.1 Vascular TE

TE is a multidisciplinary field that applies the principles of biology and engineering in order to develop tissue substitutes to restore, maintain, or improve the function of diseased or damaged human tissues when the body is not able to do it by itself [16].

To date TE has been successful in producing simple avascular tissues, such as skin and cartilage, which are thin enough for oxygen and other nutrients to diffuse passively through to sustain the cells within them [17]. Sufficient neovascularization in scaffold materials can be achieved through coordinated application of angiogenic factors with indicator cells types in different biomaterials [18].

Great advances have been made in identifying the biochemical factors and intracellular signaling pathways that mediate the control of the angiogenesis process.

1.6   Image Acquisition Techniques

1.6.1 Principles Acquisition Techniques in Tissue Engineering

Innovative surface and volume mesh generation techniques have recently been developed, which convert 3D imaging data, as obtained from magnetic resonance imaging (MRI), computed tomography (CT), micro-CT, synchrotron and ultrasound, directly into meshes suitable for use in physics-based simulations.

These techniques have several key advantages, including the ability to robustly

generate meshes for topologies of arbitrary complexity (such as bioscaffolds or composite micro-architectures) providing meshes in which the geometric accuracy of mesh domains is only dependent on the image accuracy and the ability for certain problems to model material inhomogeneity by assigning the properties based on image signal strength [19].

1.6.2 Computer Tomography (CT)

CT is a powerful nondestructive evaluation (NDE) technique for producing two dimensional (2D) and 3D cross-sectional images of an object from flat X-ray images. Characteristics of the internal structure of an object such as dimensions, shape, internal defects, and density are readily available from CT images. The imaging system produces a 2D shadowgraph image of the specimen just like a film radiograph [20]

1.6.3 Magnetic Resonance Imaging (MRI)

In MRI the study object is placed within a high intensity magnetic field. This causes the magnetic moments of the molecules within the object to become aligned. The object is then irradiated with pulses of low-level microwave radiation (excitation pulses) that cause some of the magnetic moments of the molecules to oscillate and re-emit microwaves after each pulse. These re-emissions are measured and stored digitally

1.6.4 Synchrotron Radiation (SR)

SR refers to an electromagnetic radiation produced when ultra-relativistic electrons circulating in a storage ring are deviated by strong magnetic fields. The storage ring consists of a succession of bending magnets and straight sections including insertion devices (**Figur**e 5) [21].

SR benefits from increased brilliance that is orders of magnitude greater than conventional X-ray sources. This improves image quality, reduces scan time, enables higher resolution and facilitates, also the use of monochromatic and tunable energy (single energy) X-rays of the beam is a key point since this condition is a basic

assumption in the theory of tomographic reconstruction [22].
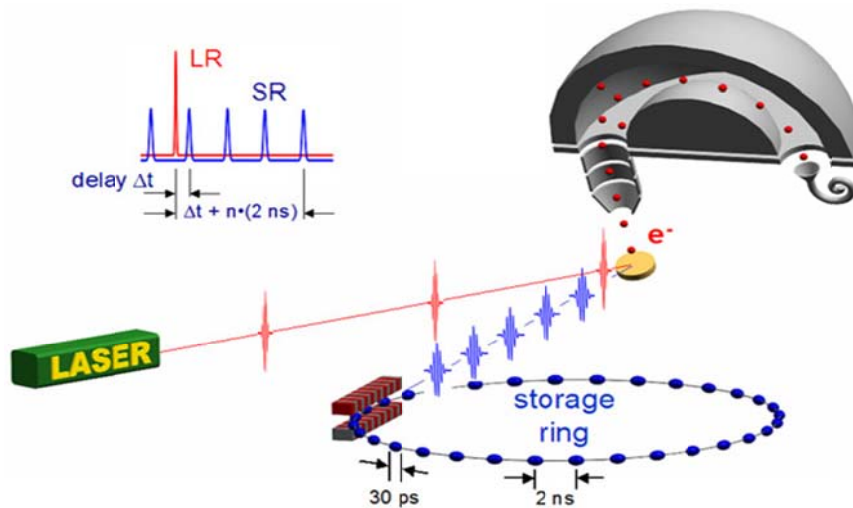
Figure 5 Synchrotron radiations scheme

1.7   Image Processing

1.7.1 Three Dimensional Image Reconstruction

3D reconstruction involves the assembly of the information contained in 2D planes of known orientation in coherent and understandable 3D images. Reconstruction of 3D geometrical models and mesh generation is also usually carried out by manual editing of the 3D model. These procedures are time-consuming and can take several days of work.

3D modeling from images for computational analysis in general requires three fundamental steps: *image segmentation, model pre-processing and mesh generation.*

In vascular applications, this process depends on the quality of the anatomic images, the complexity of the vascular and the level of expertise of the modeler [23]

In the last years, medical image processing has been introduced into clinical practice, to allow 3D visualization of anatomical structures at sub-millimetric resolution.

Image-based meshing is opening up exciting new possibilities for the application of computational mechanics methods like finite element (FE) and CFD to a wide range

of biomechanical and biomedical problems that were previously intractable owing to the difficulty in obtaining suitably and realistic models.

Data from 3D imaging modalities generally consist of a regular cartesian grid of greyscale data representing the relative signal strength throughout the scanned volume obtained from the imaging modality. The most basic step that must be carried out is segmentation, that is, the identification of volumes of interest (VOI) within the image by classification of voxels into appropriate groups. (**Figure 6**).

Volume images can be considered as 3D tables containing intensity values for particular positions in space.

| a | b | c |
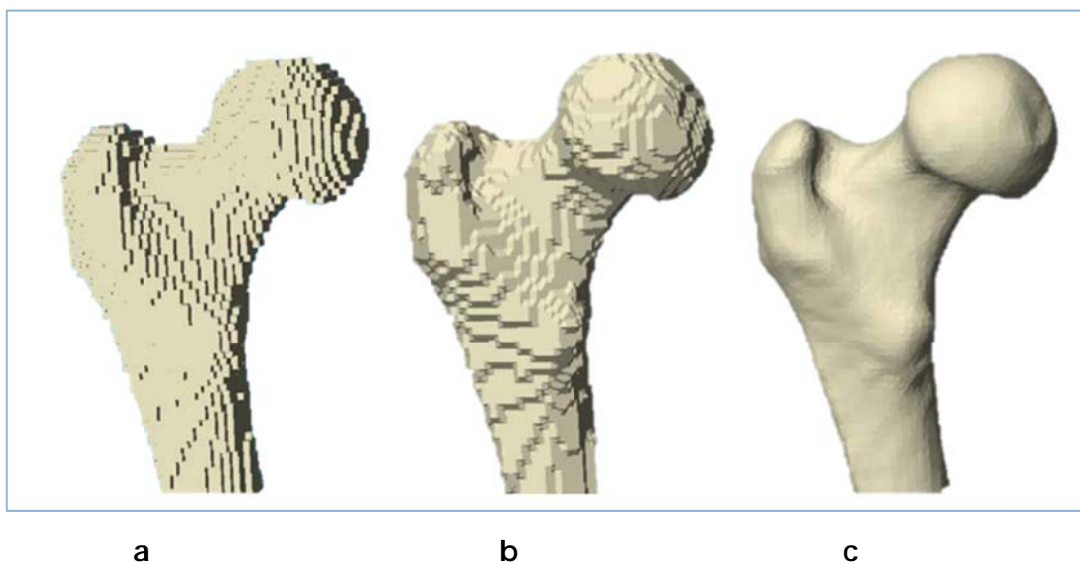
Figure 6 Reconstructions from CT scan of a dry cadaveric bone: (a) segmented volume of interest mesh, (b) surface mesh generated from marching cubes algorithm, (c) rendered view of surface mesh generated from marching cubes algorithm [24]

Background data refer to the image volume greyscale data (e.g. CT, MRI data, etc.), before and after filtering. The Segmentation of background data will then spawn one or more volumes (binary volumes) that are called Masks. These describe how an object fills the space.

A typical process outline from scan to stereolithography (STL) format, as shown on **Figure 7** would include:

- Data preparation and filtering (noise removal, resampling, cropping, etc.)

- Segmentation
- Mask filtering
- Surface extraction
- Mesh generation
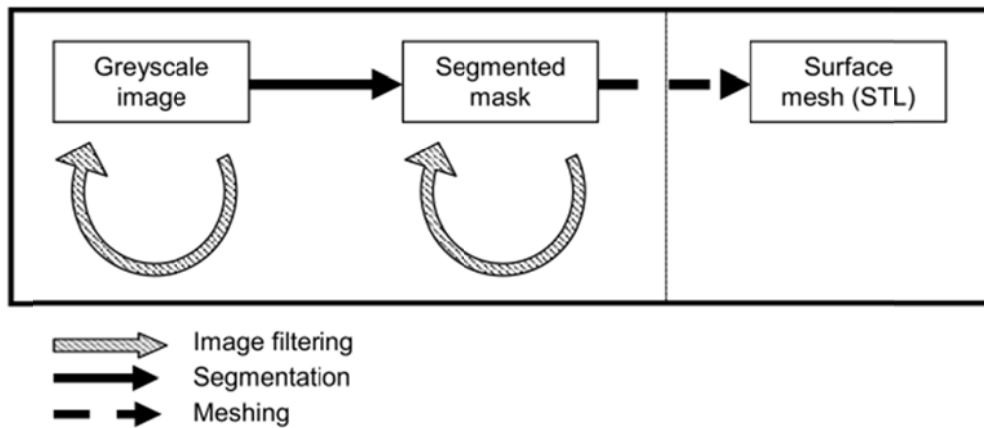
Clearly, the accuracy of any resultant model will be largely dependent on the accuracy of the initial segmentation and this will be a function not just of the image resolution but a number of other factors including noise, poor contrast between tissues and motion artefacts [19].

1.7.2 Mesh Construction

3D meshes are frequently used to perform physical simulations in science and engineering. This involves decomposing a domain into a mesh of small elements, usually with tetrahedral or hexahedral elements. Automatically creating such meshes for complicated domains is a challenging problem, especially guaranteeing good internal angles, a goal that has eluded researchers for nearly two decades [26]

The FE method is used in modeling physical phenomena of conventional and, even now, in image processing. This, by the use of volumetric meshes which are inconvenient in many cases the structure obtained does not reflect the original structure.

1.7.3 Computational Fluid Dynamics (CFD)

With the appearance of powerful and fast computers, new possibilities for replacing time-consuming model testing and field-testing have arisen. This involves solving the differential equations describing fluid motion, using either a finite volume or a FE method. These methods applied for the solution of the fluid equations of motion are named computational fluid dynamics (CFD).

CFD essentially takes the momentum, heat and mass balance equations, along with other models describing the equipment performance, and solves them to give information such as pressure, velocity and wall shear stress (WSS) profiles.

The basic principle of the CFD modeling method is that the simulated flow region is divided into small cells within each of which the flow either kept under constant conditions or varies smoothly.

In hemodynamic applications, CFD simulation of blood has been a subject of significant research effort. Over the last decade great progress has been made in computational modeling of blood flows to measure hemodynamic variables [27-29]

Chapter 2 Objective

Develop a methodology to perform a quantitative assessment of the functionality of micro-vascular networks from synchrotron and µ-CT data in two different samples, based on numerical simulation to estimate the mechanical stimulus that promote the angiogenesis process in tissue engineering constructs.

Chapter 3 Materials and Methods

The main steps used to develop the methodology to perform the CFD analysis of the vessels networks (**Figure 8**) were:

- Image acquisition

- Image segmentation and 3D reconstruction

- Superficial and solid meshes construction

- CFD analysis
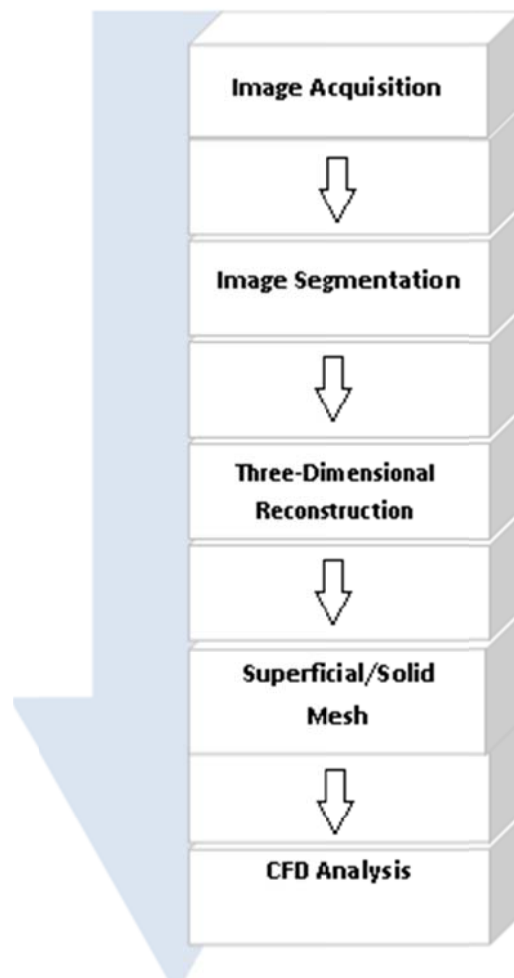
3.1   Image Acquisition

The first step to perform the computational fluid dynamic (CFD) analyses presented in this study is the image acquisition.

It was obtained by the corrosion casting method, two different samples of vessel networks formed in the tail and the lower hind limb of a mouse, provided by ETHZ from synchrotron and µCT data in DC files format.

Table 1 shows the technical acquisition specifications of each sample.

Table 1 Sample technical specifications

	Sample 1 (Tail)	Sample 2 (Limb)
Technique acquisition	Synchrotron*	micro-CT**
Resolution	1.4 µm	3 µm
Pixels	788 x 756 x1021	894 x 894 x 894
N° of DICOMS	1021	894
Slice thickness (mm)	$3{,}699219e^{-3}$	1
Sample real size (mm)	2,914x2,796x3,78	4,844x4844x4,844
Mouse section	Tail***	Limb****

*Synchrotron at the Swiss Light Source (PSI, Villigen, Switzerland)

**µCT 50 (Scanco Medical AG, Bruttisellen, Switzerland)

***Proximal part

****Lower hind limb

Figure 9 shows an overview of the image acquisition process. The image acquisition was made by the ETHZ. They have done and *In vivo* µ-computed tomography and Synchrotron radiation tomography of different mice using the corrosion casting method. They have obtained the geometry of the vessels in image slides and in DICOM format.
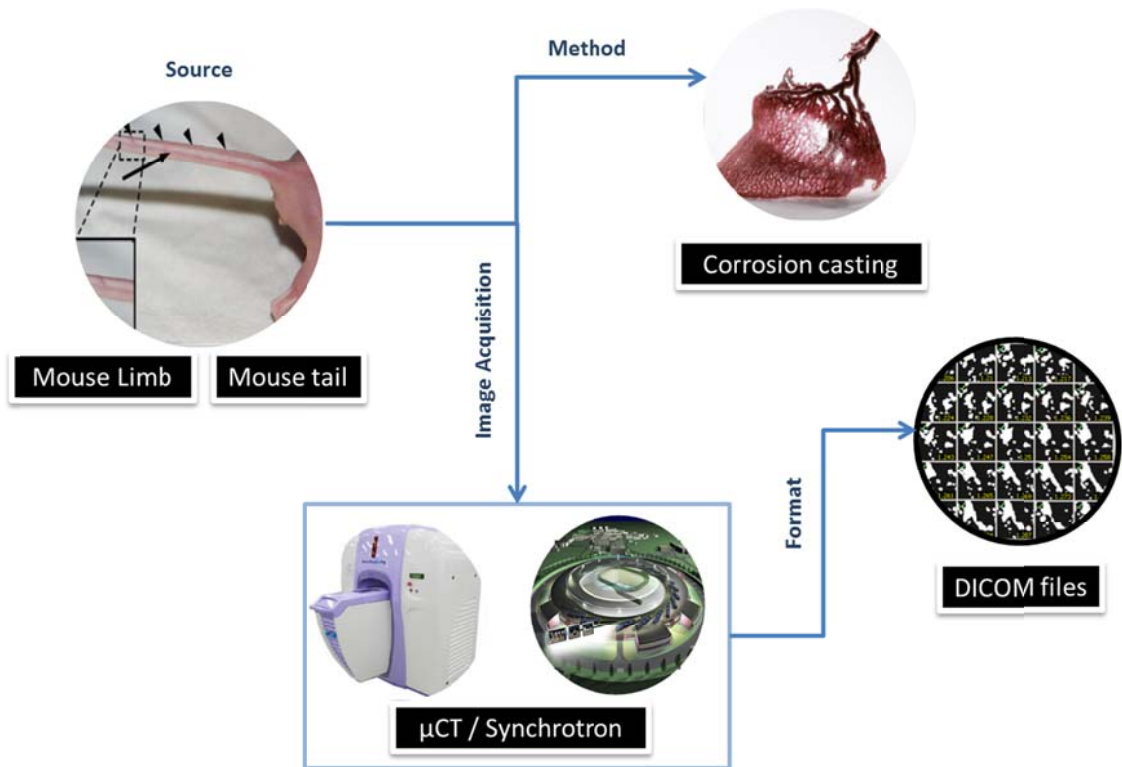
Figure 9 Image acquisition process.

The next steps to get a CFD analysis involve the 3D reconstruction of the vascular networks and the construction of a superficial and solid mesh (Figure 10).
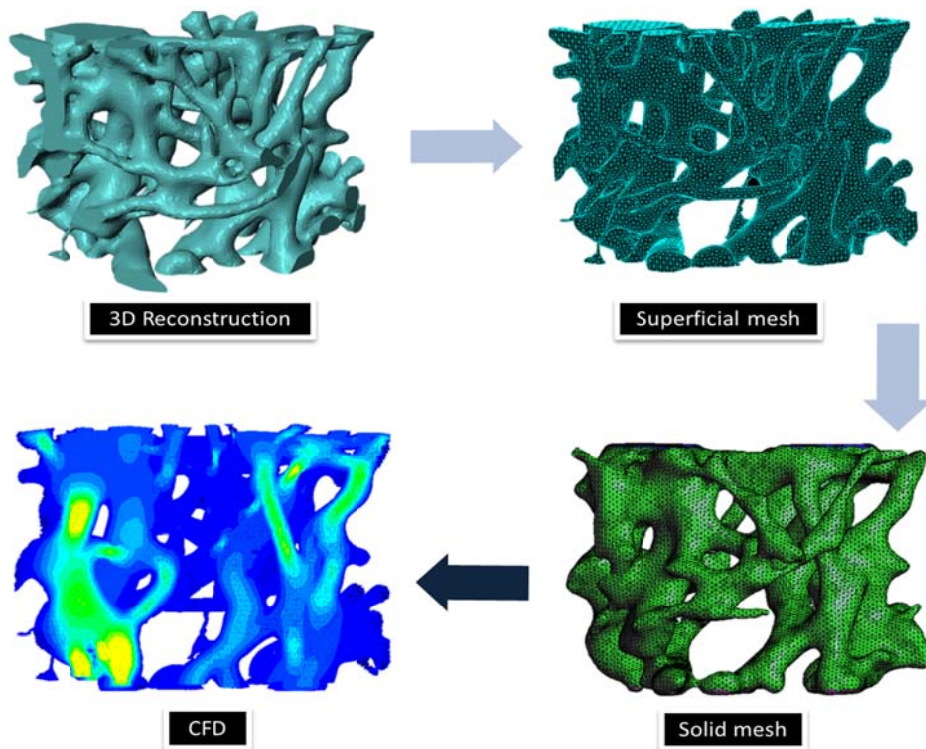
Figure 10 3D Reconstruction, superficial and solid mesh and CFD analysis (Sub-volume-Tail)

3.2   Segmentation and 3D Reconstruction

Vascular segmentation and 3D reconstruction of the vascular networks geometry were accomplished by Thresholding and FloodFill within different image processing software: MIMICS 13.1: Materialise, Haasrode, Belgium, and Simpleware 4.2: Scan IP module, United Kingdom.

The geometric models are generated from medical image data (Synchrotron and µCT data). The first step in the process of model creation is the generation of a mask that defines the region of interest (ROI). This process is known as segmentation and can be carried out manually or automatically.

By segmentation the image is divided into parts or objects that comprise it. The extent to which this subdivision is done depends on the particular application, when the segmentation process have finished, it is possible to work with the objects of interest of the application. The segmentation will lead ultimately to success or failure of the process of analysis. In most cases, a good segmentation gives rise to a right solution, so that should make every effort possible at the stage of segmentation.

In this case the segmentation process was done carefully to ensure an interconnect network. Only the connected elements of the geometry resulting of the segmentation process were used and the non-connected structures were removed to proceed with the construction of the superficial and volumetric mesh.

3.3   Superficial and Solid Mesh Construction

Once the 3D reconstructions of the networks are obtained, the next step it is to construct the triangle model of the geometries in STL format. However, these models cannot be applied by CFD packages for the generation of the required geometric mesh. One more process is needed to convert the triangle model into surface or solid model to facilitate CFD simulations.

The superficial mesh was obtained using different image processing software: MIMICS 13.1 and Simpleware (Scan IP module). And the solid or volumetric mesh

was obtained using Simpleware (Scan IP module).

Due to the large size of the data of Sample 1 (Tail), in a first step the model was divided into sections of 100 DC files to analyze the mesh density required for the full sample. At First it was analyzed the first 100 DC, then a full mesh was obtained under the required mesh density for all the DC files received applying the same condition of meshing to 6 different groups of DC: 1-500 DC, 1-600 DC, 1-700 DC, 1-800 DC, 1-900 DC, and 1-1021 DC (**Figure 11)**

Then a full mesh was obtained under the required mesh density for all the DC files received from Limb sample. Also, in order to analyze the functionality of the vascular network in more detail in tail sample, a sub-volume of 5% was taken and the same condition was applied on this sub-sample.
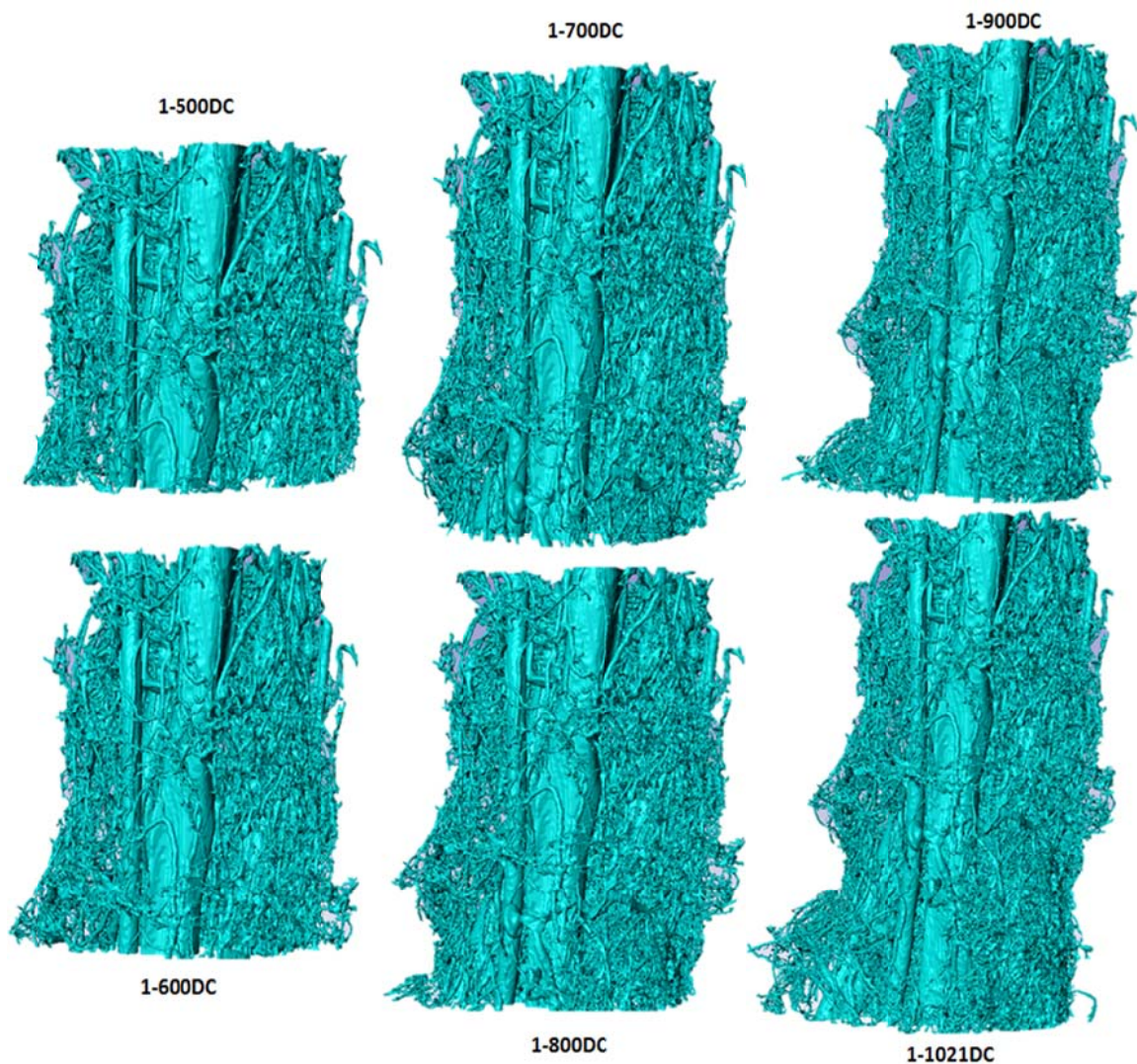
Figure 11 Full Sample Meshing

To obtain the mesh density required the "Resample" tool from Simpleware was used, which is used to reduce the size of the images by lowering resolution but without modifying sizes or features of the object. Resampling can also be useful to artificially increase the resolution by supersampling the data.

3.4 CFD Analysis

Once the mesh was obtained the CFD analysis was performed using two different commercial softwares: Ansys-Fluent 12.1 (United States) and Tdyn 11.0.5 (Spain). **Table 2** shows the properties of blood that were used [30] to simulate the fluid within the different vascular networks. It was supposed a laminar Newtonian fluid

Table 2 Blood Properties

Fluid Properties (Blood)	
Viscosity	0.0022 Kg.m-1s-1 *
Density	1060 Kg.m-3 **

The boundary conditions were defined in Fluent and Tdyn to simulate blood movement from the superior to inferior position **Table 3** shows the boundary conditions used to the CFD analysis in the samples. The velocity was applied in the superior region of the networks and the pressure outlet was applied in the inferior region of the network **(Figure 12)**.

Table 3 Boundary Conditions

Boundary Conditions	
Velocity (inlet)	1 mm s-1
Pressure (Outlet)	0 Pa
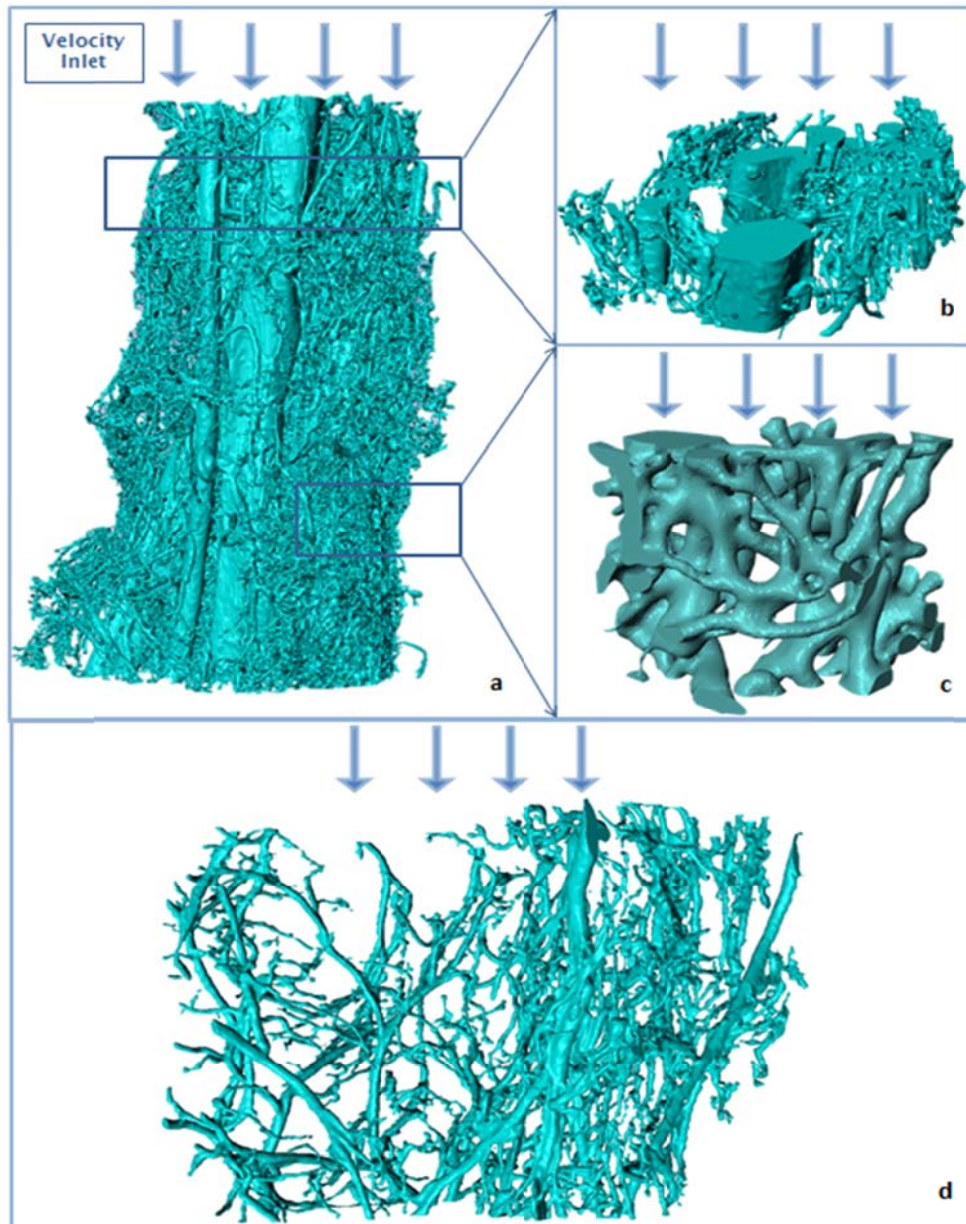
Figure 12 Boundary conditions. a. Tail, b. Sub-volume Tail (10%), c. Sub volume Tail (5%), d. Limb

Chapter 4 Results

4.1   Reconstruction Analysis:

The results obtained from the segmentation process of the two samples are shown in **Figure 13**. We obtained two different masks: the red mask contained the preliminary segmentation of the vascular networks, that include the entire geometry of the sample, and the green mask shows the segmentation of the images containing only connected structures in the vascular network.
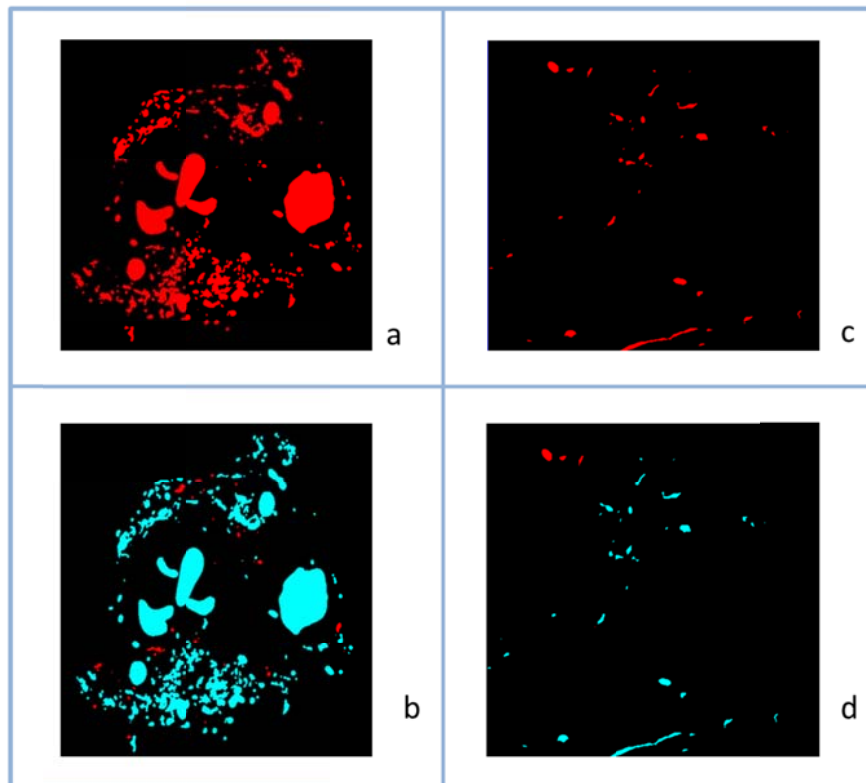
Figure 13 Segmentations process using Simpleware Software. a and b. Tail, c and d. Limb.

To obtain the red mask it is necessary to use the Threshold tool to make sure that the entire geometry is reconstructed without losing any important segment of the vascular networks. And to obtain the green mask in the segmentation process it was used the Floodfild tool to eliminate the structures that were not connected to the main model.

The results of the 3D reconstruction of the interconnected vascular network and the real size of the two samples are shown in **Figure 14**. The volume of both structures was preserved almost entirely.
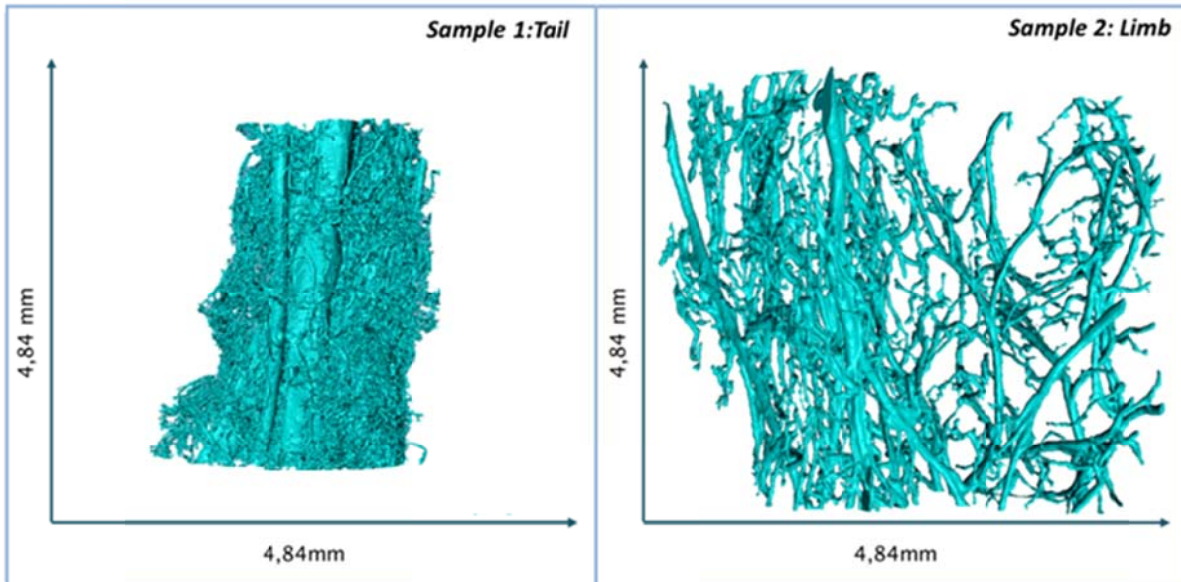
Figure 14 3D Reconstruction of vascular networks interconnected using Simpleware. Software

Table 4 shows the result of the volume obtained from the segmentation and 3D reconstructions process of the two samples with their non-connected and connected segments.

Table 4 Volume result of segmentation and 3D reconstruction process

	Sample 1	Sample 2
Volume mask red (mm³)	2,288	1,630
Volume mask green (mm³)	2,284	1,570
Difference volume (%)	0,174	3,681

The percentage of difference between the volume of non-connected and connected structure in Sample 1 is 0,1748% which correspond to an improved segmentation process with a large volume of interconnected structure.

The difference of volume in the Sample 2 is a lit bit higher (3,681%). This loss of volume is possible because this Sample is a sub-selection of a bigger one, and some of the reconstructed geometry structures belong to this complete sample.

4.2   Superficial and Solid Mesh Construction

During the reconstruction process we find some drawbacks, for example, the software MIMICS have limitations in the three-dimensional reconstruction of the superficial mesh as problems with the quality of the generated mesh and the number of elements on the surface and solid mesh were found, mainly with the large samples with a big amount of DC files.

Using the Sample 1 as example, it was obtained a volumetric mesh with around 50 10^9 elements (**Table 5**) with many flipped elements and with a huge loss of the geometry from the original model. These cause problems for graphic processing and huge amount of memory Random-access memory (RAM) and Central Processing Unit (CPU).

Also to improve the superficial mesh with MIMICS it is necessary a long time of analysis, that makes more inefficient applied the same protocol with another samples.

The superficial mesh obtained using MIMICS from a sub-volume of tail Sample is shown in **Figure 15**. Here we can see the flipped elements, the bad contours, and also a bad non-smoothing surface, which do not allow us to continue the CFD analysis according to our requirements.
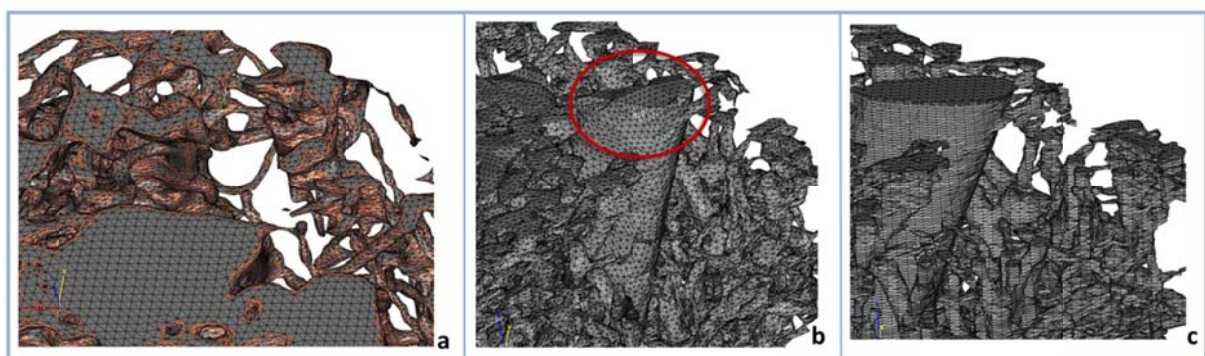
Figure 15 Superficial mesh (Sample 1 segment) using MIMICS. a.Bad triangles in orange, b. and c. shows a non-smoothing surface and the loss of important components of geometry

Table 5 Tail sample: Elements and nodes in superficial and solid mesh using MIMICS

	Mesh type	Elements	Nodes
Sample 1	Superficial	5.595.500.000	2.764.300.000
	Solid (Tetrahedral)	50.080.500.000	9.492.700.729

Due to the limitations exposed previously with MIMICS, only Simpleware was used to develop this methodology. Simpleware was used in the segmentation process, 3D reconstruction, superficial and solid meshing.

The software used in each stage of building the methodology for CFD analysis is shown in **Figure 16**.

Figure 16 Software used in the methodology developing

With Simpleware were obtained the superficial mesh of the two samples (**Figure 17**). Due to visualization limitations, the complete tail and limb meshing are not shown here, because of the number of elements it is not possible to differentiate the entire structure in both samples.

Table 6 shows the features of the superficial mesh obtained from tail and limb samples.

Table 6 Superficial mesh features

Superficial mesh	Sample 1	Sample 2
Elements	42.706.038	9.389.792
Nodes	22.647.252	4.134.232
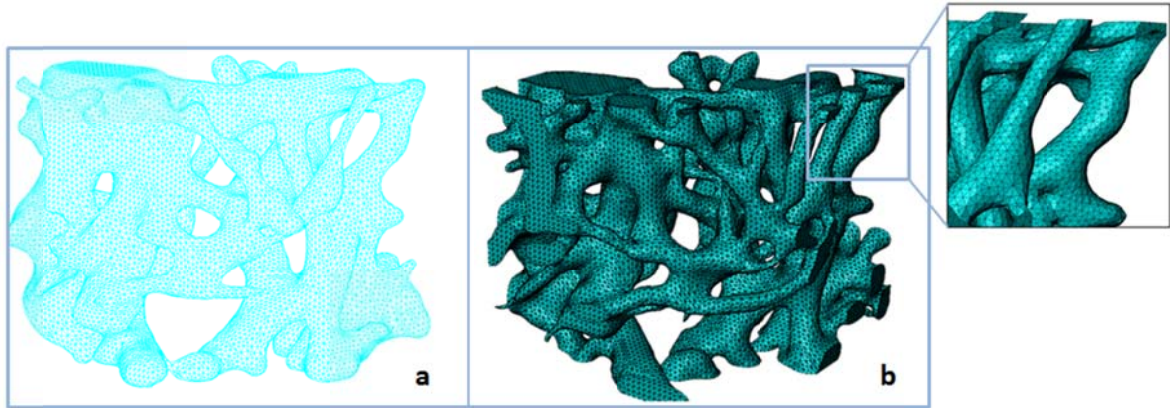
Figure 17 Sample 1 sub-volume. a. Superficial mesh, b. Solid mesh

4.3   Mesh density requirement

The 3D reconstruction is the process through which real objects are reproduced in the computer memory, maintaining their physical characteristics (size, shape and volume). The efficiency of the algorithm is what defines the quality of the final mesh. Assuming a set of points misrepresented, there will be points that do not meet defined optimal conditions for meshing.

The points are very close to each other, the noisy points and redundant points, offer no information for reconstruction

In our case, three-dimensional reconstruction is performed based the large size of the Sample 1; in a first step the model was divided into sections of 100 Dicom files to analyses the mesh density required for the full sample. The mesh optimization was made in the first 100DC at the top of the Sample 1.

The Frontal and isometric view of Tail Sample DICOMCS fragmentation can be seen in **Figure 18**.
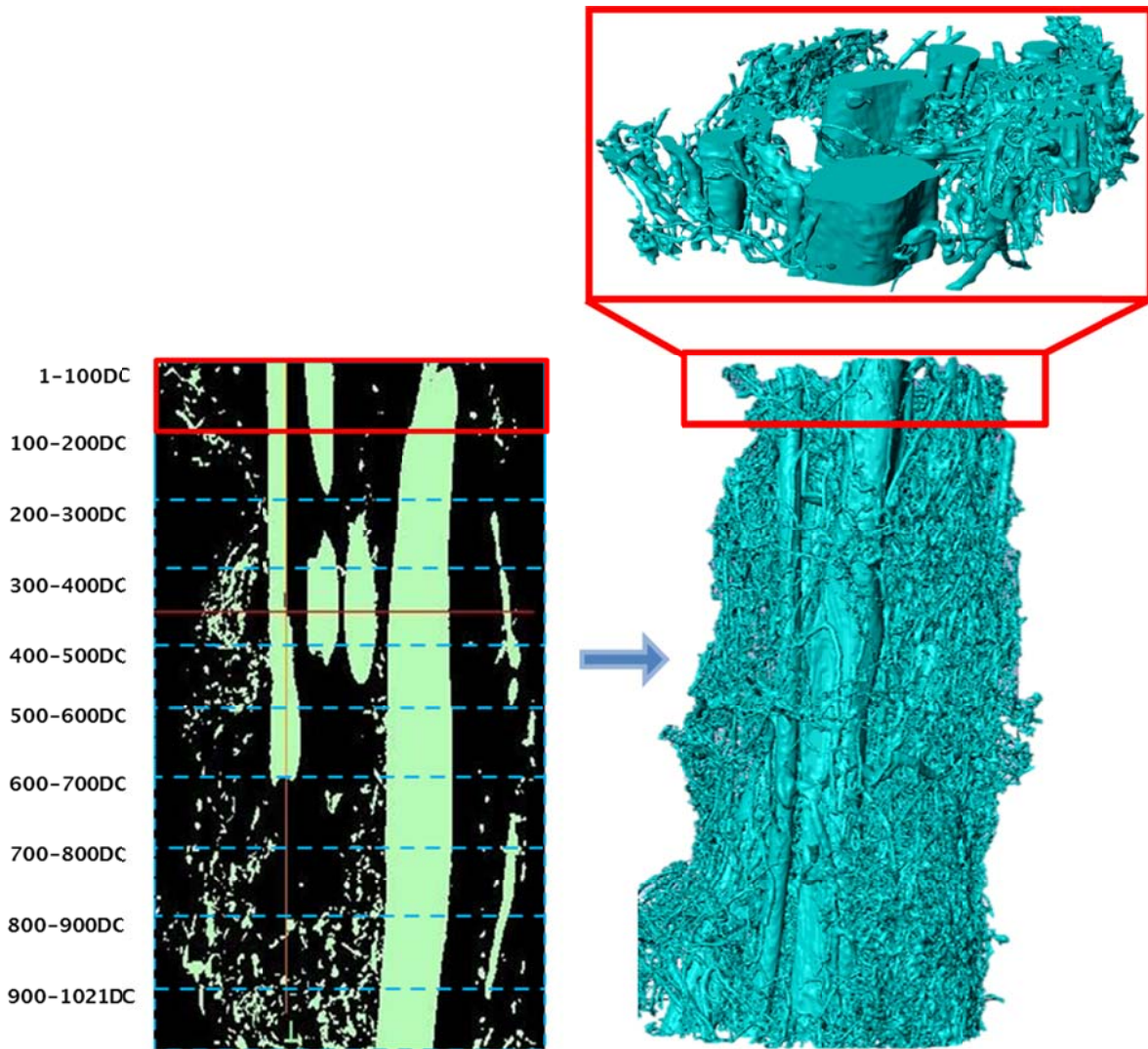
Figure 18 Frontal and isometric view of Sample 1 (DC fragmentation)

The meshing used is tetrahedral and hexahedral meshes because they are shielded from volumetric reconstruction, as opposed to triangular meshes as we provide information about superficial aspects of the 3D structures. Therefore, both types of mesh are not mutually each exclusive, fate complementary allowing the reconstruction of complex solid structures.

The aim to achieve is the collection of structures that have as much possible information, and turn, the mesh too much simple data, preventing acute angle and/or too much information on the structure, this avoids a greater analysis time. In our case, meshing with optimum results in the mesh tetrahedral because it has the best results in this study because it is the most commonly used in CFD analysis.

In brief, two types of meshes with different elements were analyzed. Meshes with only tetrahedral elements and meshes with a mixture of tetrahedral and hexahedral elements were obtained. In both cases the mesh density was varied parametrically in order to find the best compromise between calculation time and accuracy of the CFD analysis (**Figure 19**).

a

b
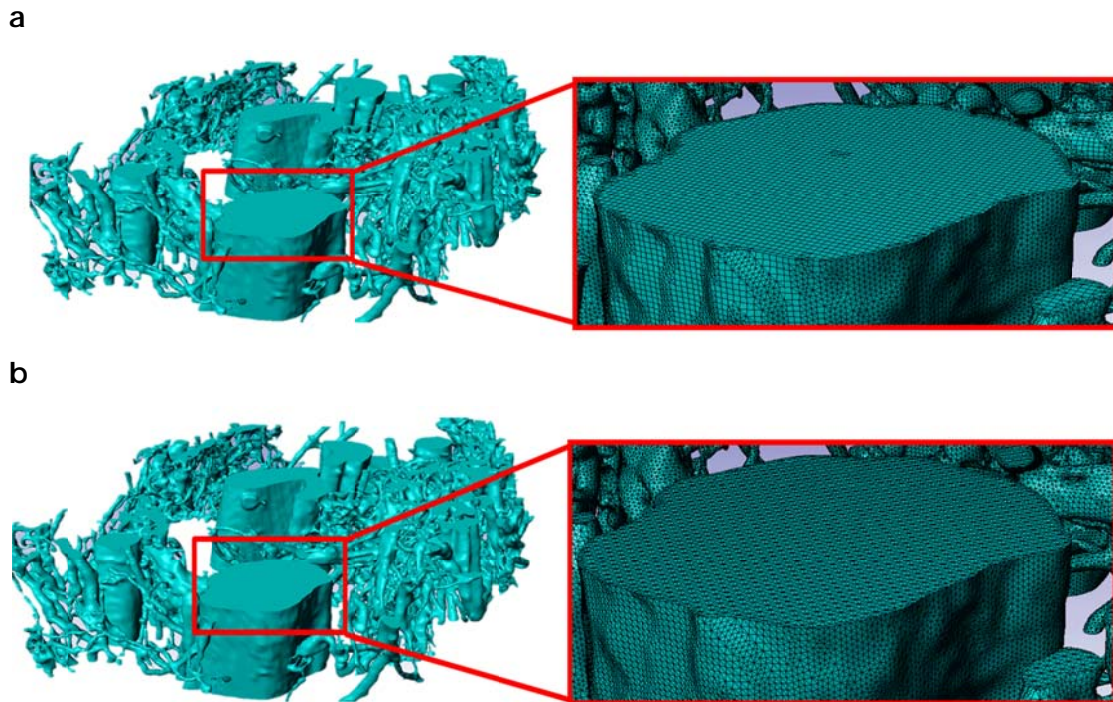
Figure 19. 100 DC Solid mesh section from the tail sample. a. Tetrahedral and hexahedral mesh. b. Tetrahedral mesh.

In order to obtain an adequate mesh density without losing important features of the vascular networks, it was applied different values of resample in both types of mesh and the quality of the elements was verified at each point of resample.

It was used values of resampling from 1 (without resample - w/o) to 2 times resample, and it was obtained two meshes from each case (Tetrahedral and a mixture of tetrahedral and hexahedral elements)

The number of elements and nodes and the volume obtained for each type of mesh (Tetrahedral and a mixture of tetrahedral and hexahedral elements) in the first 100DC segment are shown in **Figure 20**.
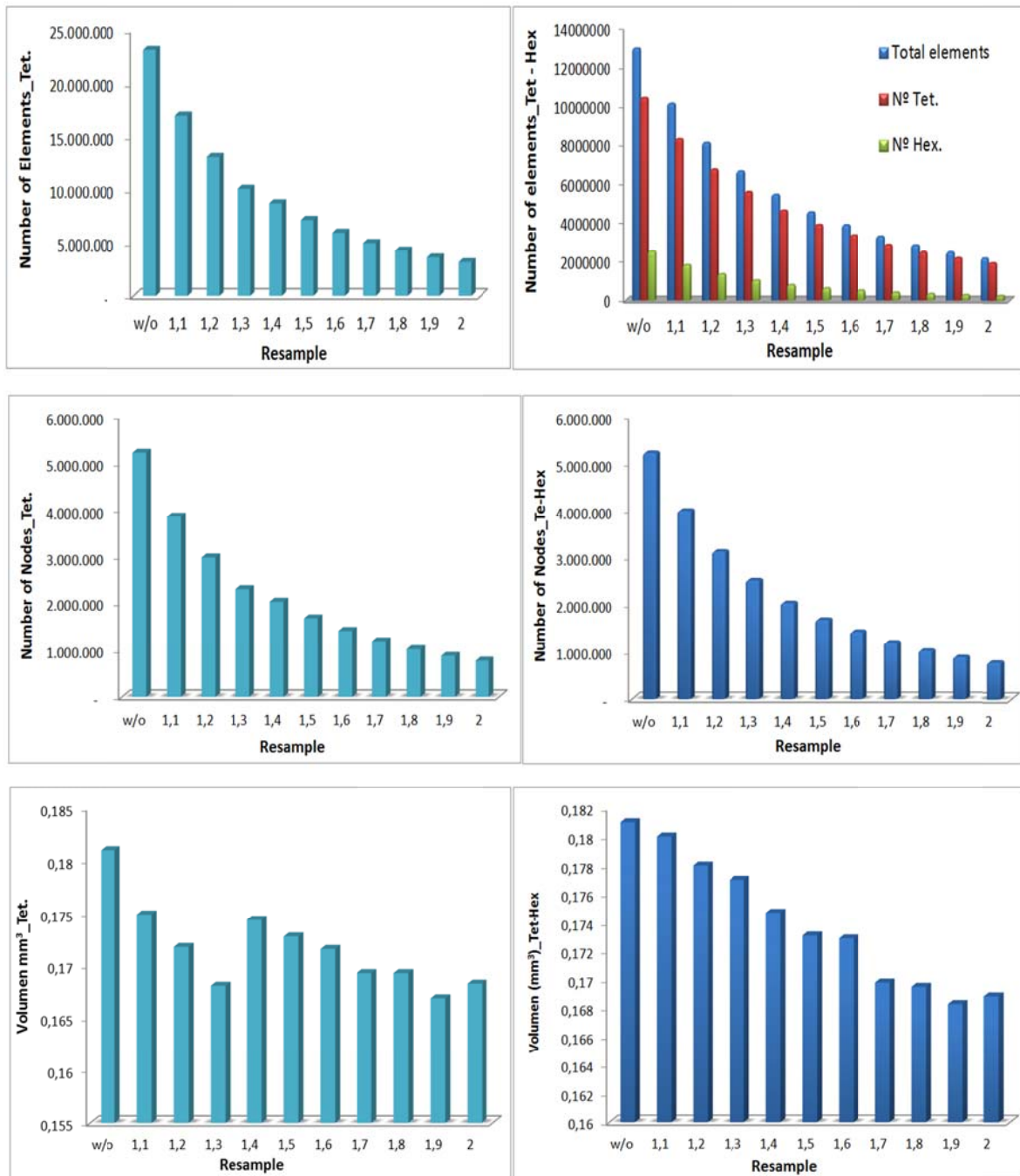
Figure 20 Number of elements, nodes and volume for two types of mesh to analyze the mesh density require

The numbers of elements decrease in both types of meshes when the value of resampling increases.

The mixed tetrahedral and hexahedral mesh, reaches a lower number of elements of both meshes at resample from 2 times, passing to 12 million to 2 million of elements (**Table 7**).

In both types of meshes, the number of nodes decrease when the value of resampling increase in a similar way. Both cases pass to 5 million (without resample) to around 700,000 nodes at resample from 2 times (**Table 7**, **Table 8**).

Table 7 Results Resample. Tet_Hex Mesh

DICOMS	Resample	Number ele.	N° Tet	N° Hex	Nodes	Volumen (mm³)
	W/O	12.965.527	10.434.756	2.530.771	5.227.177	1,89E-01
	1,1	10.139.959	8.302.720	1.837.239	3.992.863	1,88E-01
	1,2	8.110.333	6.744.622	1.365.711	3.127.902	1,78E-01
	1,3	6.644.638	5.593.585	1.051.053	2.522.301	1,88E-01
	1,4	5.445.852	4.634.108	811.744	2.038.914	1,86E-01
1-100	1,5	4.544.994	3.900.913	644.081	1.684.046	1,86E-01
	1,6	3.885.296	3.359.525	525.871	1.430.184	1,88E-01
	1,7	3.297.241	2.874.161	423.080	1.201.527	1,86E-01
	1,8	2.850.326	2.499.305	351.021	1.031.512	1,87E-01
	1,9	2.491.161	2.199.341	291.820	894.803	1,87E-01
	2	2.204.834	1.957.575	247.259	786.397	1,89E-01

Table 8 Result Resamples. Tet_Mesh

DICOMS	Resample	Elements	Nodes	Volumen (mm³)
	W/O	23.149.531	5.227.177	1,89E-01
	1,1	16.995.056	3.852.017	1,80E-01
	1,2	13.060.842	2.982.006	1,78E-01
	1,3	10.089.351	2.307.677	1,74E-01
	1,4	8.717.743	2.038.914	1,88E-01
1-100	1,5	7.142.543	1.684.046	1,86E-01
	1,6	5.948.193	1.414.231	1,87E-01
	1,7	4.978.765	1.193.347	1,86E-01
	1,8	4.252.708	1.027.209	1,87E-01
	1,9	3.629.084	883.920	1,86E-01
	2	3.184.789	780.818	1,89E-01

It was verified that volume was kept constant whatever the amount of mesh density and the type of element mesh. In both cases the volume remained constant with small differences between the values obtained, ranging from 0,174 mm³ to 0,189 mm³.

It was necessary to check the mesh quality in both cases to ensure the accuracy of the results to decide the mesh density used to perform the CFD analysis. The quality of a mesh depends on the quality of its elements, which in turn depends on the application.

Figure 21 shows the mesh quality of both types of meshes obtained. The mesh quality in this study is related with two important elements aspect ratio:

- **In-out aspect ratio** gives a robust estimation of the quality of the elements when used for finite element analysis. Since elements with poor aspect ratio can lead to numerical problems in these analyses, high quality elements are an important feature of the mesh.

- **The edge length ratio** also provides a measure of the distortion of the element from equilateral. Higher values indicate poorer elements.

The resample of 1.6 times has better mesh quality than the others results in both meshes, suggesting these resampling conditions as optimal to the construction of the superficial and solid mesh in both samples.
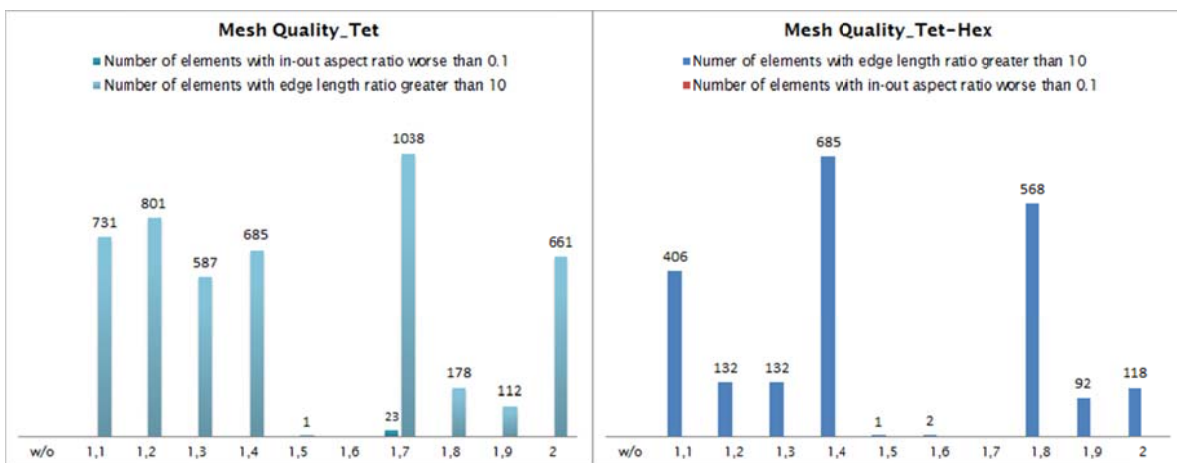
Figure 21 Mesh quality Tet and Tet-Hex elements.

Finally, results indicated that the optimized mesh for the tetrahedral model was obtained with 5,948,193 elements and 1,414,231 nodes. For the model with a mixture of tetrahedral and hexahedral elements, 3,885,296 elements and 1,430,184 nodes were necessary.

The CFD analysis in Fluent indicated that both models gave very similar fluid flow distribution. It was decided to use tetrahedral meshes in both samples, because it is shown that CFD simulations are more accurate and precise if tetrahedral elements are used instead of a mixture of tetrahedral and hexahedral elements. Accurately generating robust tetrahedral meshes is an important step and deserves particular

consideration to the necessary mathematics involved.

The number of elements, nodes, the volume and the mesh quality obtained for the tetrahedral mesh of the full tail sample are shown in **Figure 22 a**nd **Table 9**.
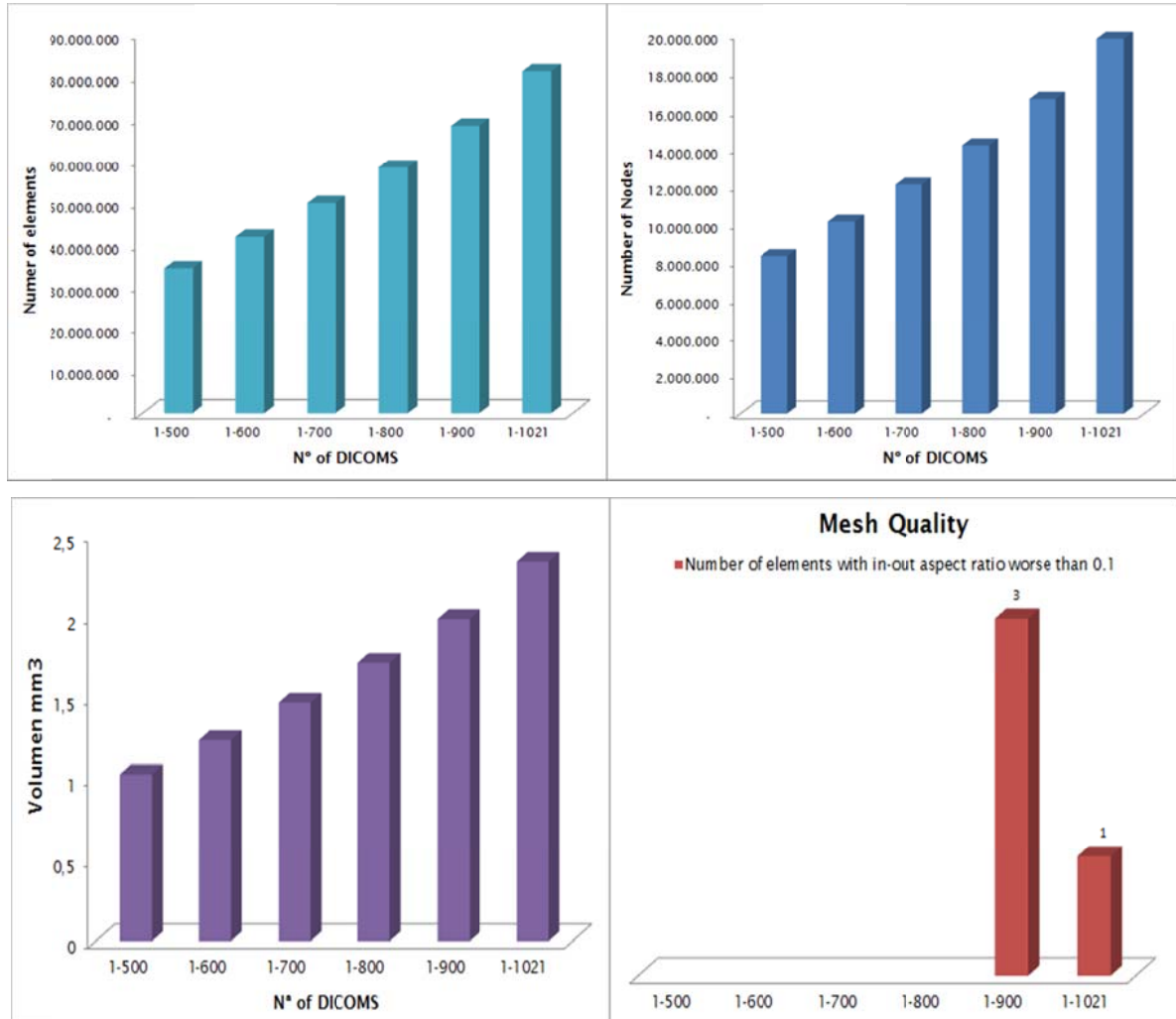
Figure 22 Full sample meshing. Number of elements, nodes, volume, and quality of the mesh

Table 9 Full sample meshing

	N° DICOMS	Elements	Nodes	Volume (mm³)
Resample 1,6	1-500	34.553.099	8.337.505	1,03
	1-600	41.923.895	10.135.918	1,24
	1-700	49.980.991	12.107.533	1,47
	1-800	58.522.515	14.200.748	1,72
	1-900	68.453.367	16.650.652	1,99
	1-1021	81.250.605	19.781.737	2,34

The results were as expected in the full model, according to the analysis described above and applying the same conditions to optimize the mesh according to the results section 100DC. You can see a direct relationship between the number of DC and the number of elements, nodes and volume, indicating that the greater the number of DC increased vascular network complexity analysis for our respective

Finally, the same conditions obtained from this parametric study were applied to the limb sample. **Figure 23** shows the differences between the number of elements, nodes, and volume obtained without (w/o) resampling and with a resampling of 1.6 times.
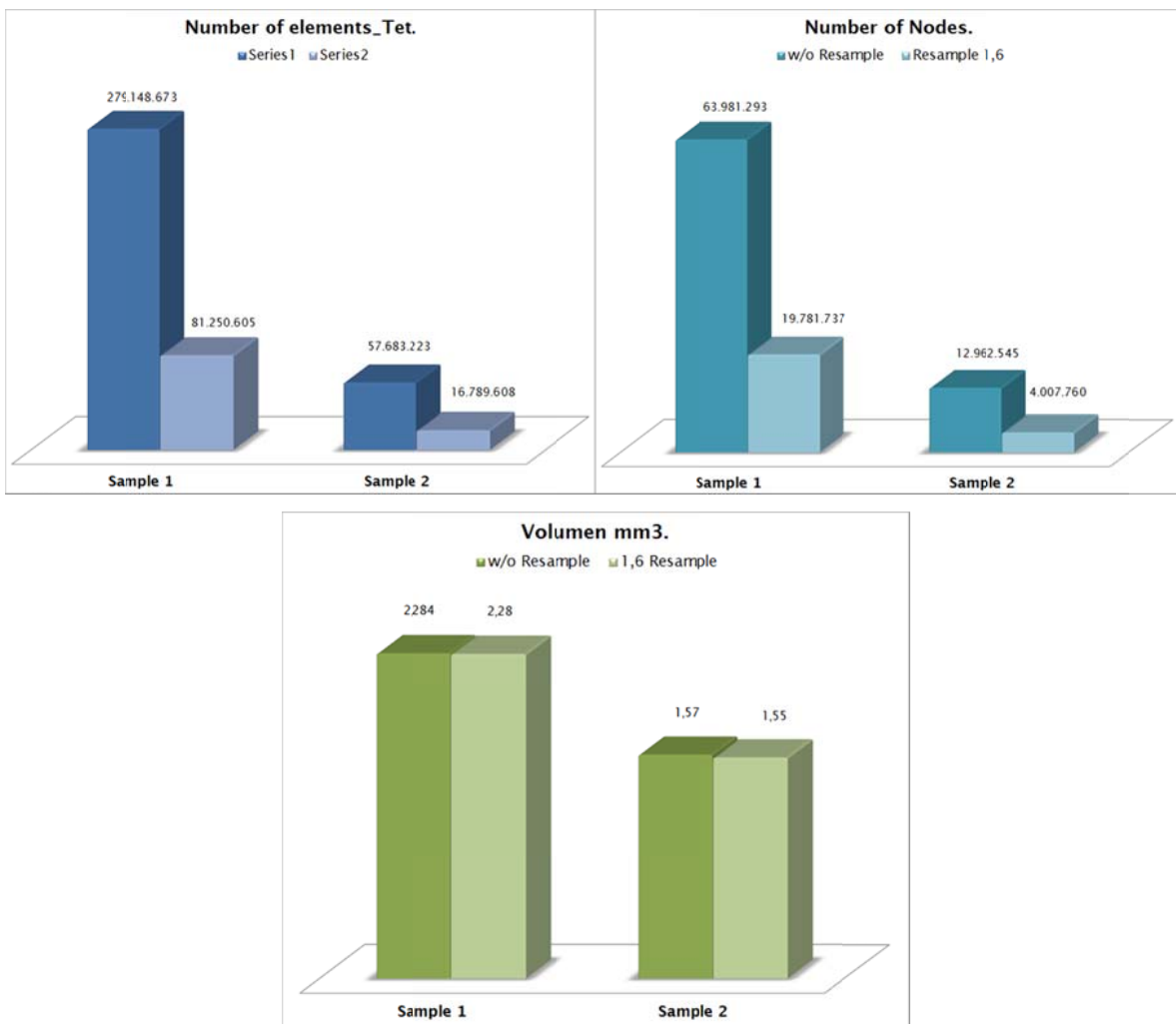
Figure 23 Number of elements, nodes, and volume from solid mesh (Sample 1 and 2)

A full tetrahedral mesh was obtained with 81 million of elements, and 19 million of nodes without loss of volume of structures futures (0,175% of loss volume) with a

resample of 1.6 times with a reduction of 71% of elements and 69% of nodes density in the full sample 1 (tail).

With the limb sample, a full tetrahedral mesh was obtained with 16 million of elements, and 4 millions of nodes without loss of volume of structures futures (1,27) with a resample of 1.6 times with a reduction of 71% of elements and 69% of nodes density in the full limb sample .**Table 10**

Table 10 Elements, nodes, and volume values (Tail and limb samples)

		Elements	Nodes	Volume (mm³)
w/o Resample	Sample 1	279.148.673	63.981.293	2,28
	Sample 2	57.683.223	12.962.545	1,58
Resample 1,6	Sample 1	81.250.605	19.781.737	2,28
	Sample 2	16.789.608	4.007.760	1,55
Reduction (%)	Sample 1	71	69	0,17
	Sample 2	71	69	1,27

4.4   CFD Analysis

4.4.1 Tail sample

4.4.1.1   Sub-volume (5%)

In order to better understand the behavior of the vascular network of tail sample, it was extracted a volume corresponding to 5% and it was analyzed the results of blood velocity and WSS. In this case we used the same boundary condition proposed above.

Using CFD analysis, we visualized velocity profiles and calculated wall shear stress along the vessels wall.

I.   Velocity profile

The velocity profile of this network shows a distribution of fluid flow on different planes. We can see the heterogeneity of fluid flow distribution in the vessels, and the direction of the blood movement. This is the highest velocity is 3 times higher

than the inlet velocity.

Velocity values inside the vessels range from 1 to 3 m.s^{-1} (**Figure 24**) Also we can observe changes in the vascular network velocity with the change in size of the vascular sections. For example we can see that increasing the vessel diameter, the velocity decreases in this section and, in the region with a small diameter an increase in the velocity was observed. Finally it was observed in some vessels a velocity equals to zero.
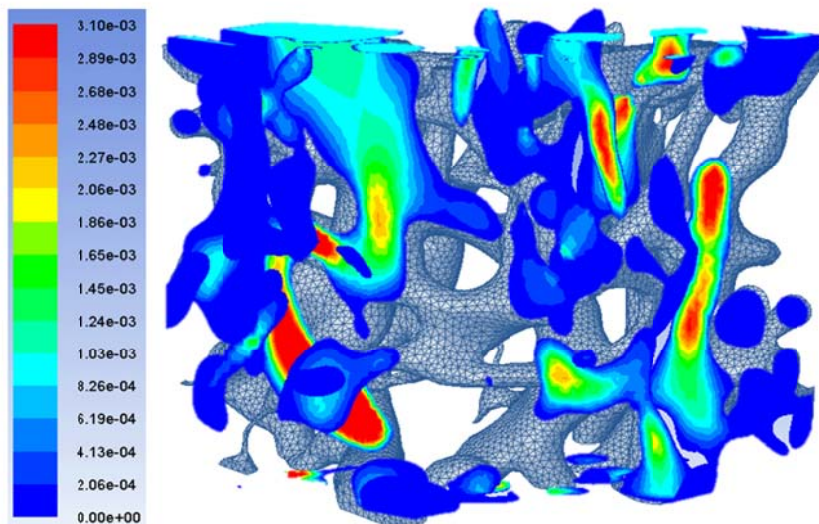
Figure 24 Contours of Velocity magnitude (m.s^{-1}) (5% of Tail sample)

In conclusion, the velocity profile of this network shows a distribution of fluid flow a in a 2D cross-section. We can see the heterogeneity of fluid flow distribution in the vessels, and the direction of the blood's movement. This is a scale of 3 times the velocity inlet.

II. Wall Shear Stress

Figure 25 shows the distribution of the wall shear stress (WSS) in the tail sample sub-volume, with a maximum value of 1.039 Pa and a distribution inside one of the large vessels with values around to 0.5 Pa.
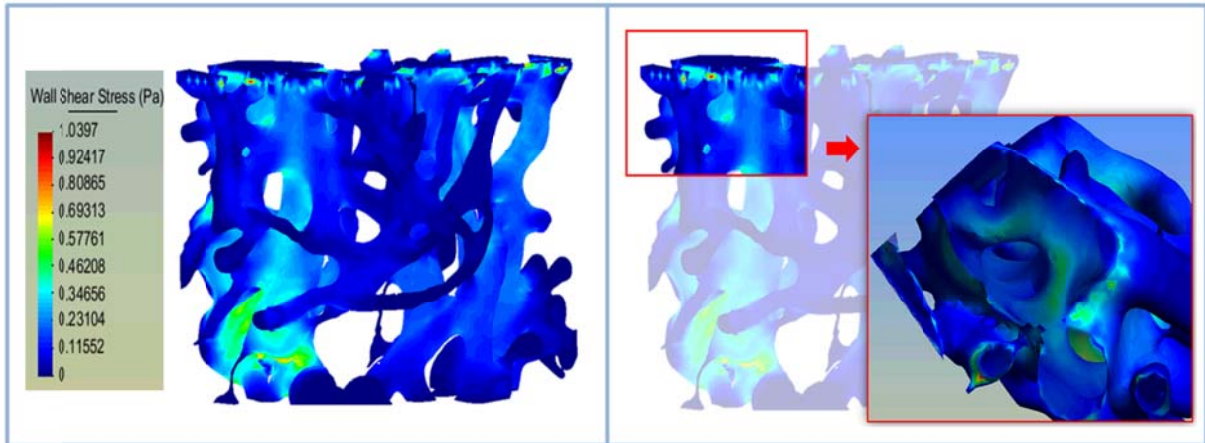
Figure 25. Distribution of WSS (5% Tail sample)

4.4.1.2 Sub-volume (10%)-100 DICOMS

Here we can see the results for the two types of meshes obtained in the optimization process described above (Section 3.3 Mesh Density Requires).

I. Velocity profile
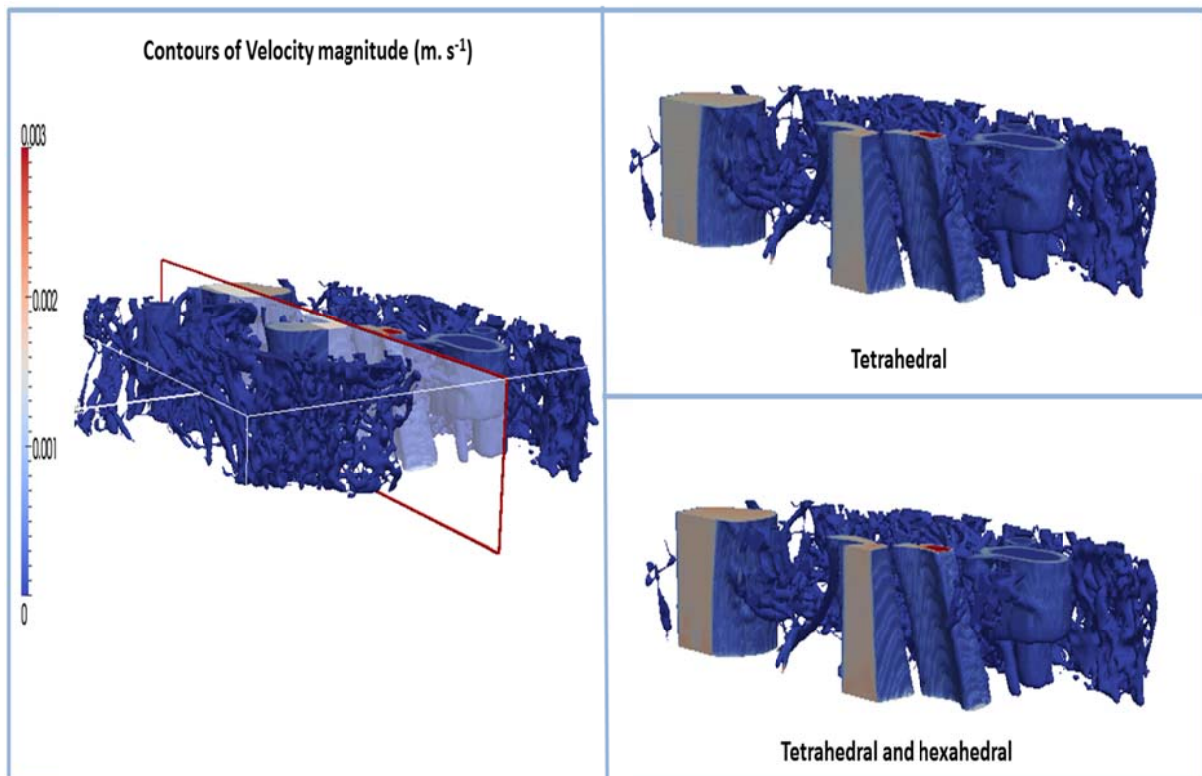
Figure 26 Contours of Velocity magnitude (m.s^{-1}) (10% of Sample 1)_Tetrahedral and mixture of Tetrahedral an hexahedral mesh

Velocity values inside the vessels range from 1 and 3 m.s^{-1}. As it was showed in the Sample 1 sub-volume of 5%, in some vessels the velocity is equal to zero.

To perform the CFD analysis we have used a Window Server 2008 R2 Enterprise with two processors Intel (R) Xeon(R) 3GHz and 48GB of memory RAM. Finally it was observed similar qualitatively results in the CFD analysis of these two meshes; we decided to use tetrahedral elements to perform the CFD analysis of the other samples.

4.4.1.3 Full Sample

I. Velocity profile

The velocity profile of this network shows a distribution of fluid flow on different planes. (**Figur**e 27) We can see the heterogeneity of fluid flow distribution in the vessels, and the direction of the blood's movement. This is a scale of 3 times the velocity inlet.

Velocity values inside the vessels range from 1 and 3 m. s-1. As it was showed in 5% and 10% sub-volume, in some vessels the velocity is equal to zero, mainly in the small lateral vessels.

It was observed that the velocity is higher inside the small capillaries than the larger ones.
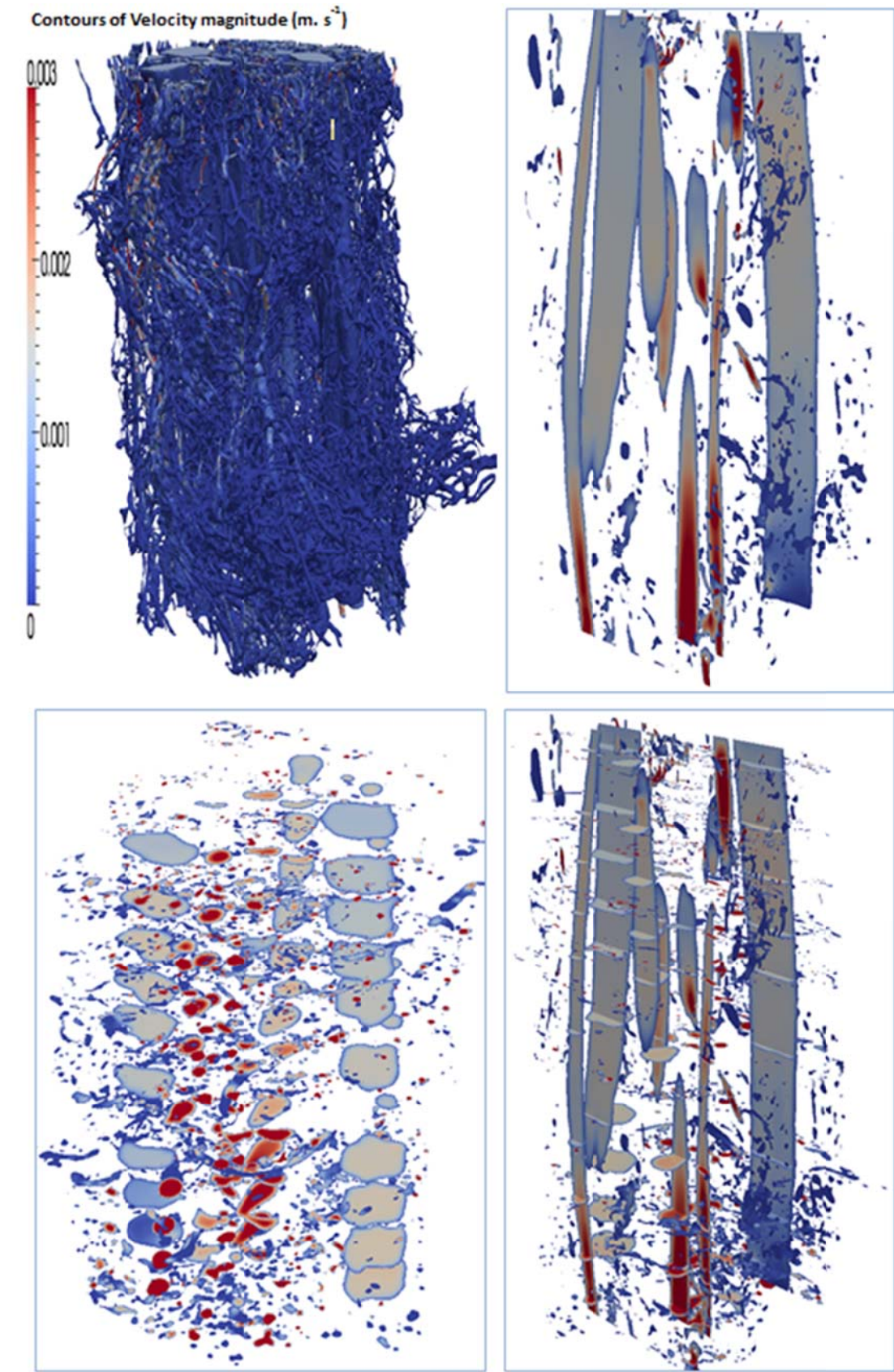
Figure 27 Contours of Velocity magnitude (m. s-1) Sample 1

4.4.2 Limb sample

I. Velocity profile

Contours of Velocity magnitude (m. s⁻¹)
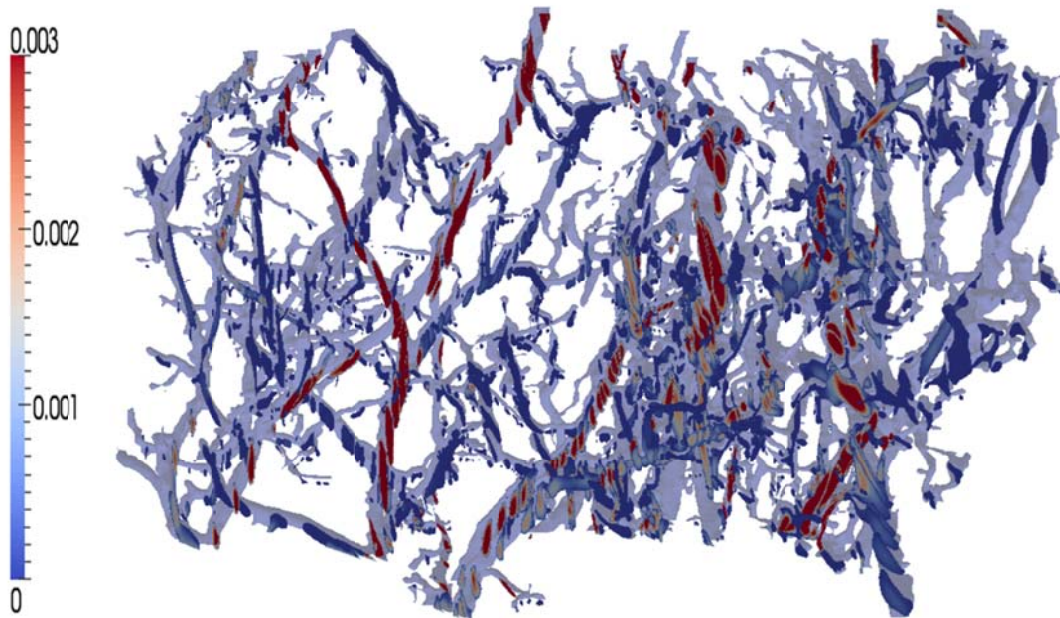
Figure 28 Contours of Velocity magnitude (m. s-1). Sample 2

The velocity profile of this network shows a distribution of fluid flow on different planes (**Figur**e **28)**. We can see the heterogeneity of fluid flow distribution in the vessels, and the direction of the blood's movement. This is a scale of 3 times the velocity inlet.

Velocity values inside the vessels range from 1 and 3 m. s-1.

As it was showed in Sample 1, in some vessels the velocity is equal to zero In this network the vessels are not well connected, maybe that is why a big percentage of the volume have velocity equal to zero.

The methodology for automated mesh generation described in the previous Section has one potential limitation, the fact that the computational mesh is generated on the basis of the geometry, and not on the basis of the expected flow features.

Chapter 5 Discussion and Limitations

5.1   Discussion

In the velocity results in both samples, it was observed in some vessels a velocity equals to zero. This possibly means that these vessels are not well trained and connected to the rest of the network, and the blood cannot pass through these vessels. Theoretically the cells that surround these "non-functional" vessels do not receive the nutrients and oxygen from the blood necessary to survive.

The values of WSS obtained with the CFD analysis were within the physiological range found in the human body reported in literature [36]. There is a vast amount of experimental evidence demonstrating that externally applied mechanical stresses (fluid shear stress, stretch, and pressure) regulate cytoskeletal organization, signal transduction, gene expression, and a wide variety of EC functions, including migration, proliferation, and ECM remodeling, which suggests a role of extrinsic stresses in angiogenesis.

In fact, many studies have shown that fluid shear stress and stretch can affect the production and/or activity of the endogenous biochemical factors, although most of these investigations were not conducted in the context of angiogenesis. [9]

With numerical simulations we can measure the WSS in each point of the network and we can predict that the cells surround this vessels could be stimulated mechanically and in response to this stimulus, the angiogenesis process could be continue.

This is a promising study that involves concurrent research groups either by analyzing the profiles of cellular and molecular biology of the process of angiogenesis, another investigation group the process behind the regenerative engineering of angiogenesis in the physiological phenomena and we systematizing the study as a computational model and its potential applications in improving the understanding of the process of new blood vessels.

5.2   Limitations

Some limitations were found in the development of this project.

Both the time meshing as the CFD analysis time was quite long due to the density and quality of the mesh required in both samples. To make starting the simulation it was required the use of servers with special technical features.

On the other hand, the results of CFD analysis cannot be interpreted entirely as a physiological behavior, since the boundary conditions were imposed on the development of the methodology does not correspond to "real" conditions in both samples, because in the process of image acquisition, was not taken into account the position of the sample, which could not be identified clearly the direction of movement of the blood.

In addition, the samples that were sent to us to perform the CFD analysis correspond to sub-groups of larger samples, so it may have been lost of information from the actual geometry of both samples.

Similarly, the method used for the acquisition of such data (corrosion casting) have certain limitations when it comes to micro-capillary samples, like in this case, since the polymer sometimes fails to fully invade the vessels and the images acquired reported vessels not connected when it really should be in the original sample.

It is also important to note that our computational simulation treated the blood as a Newtonian fluid and discounted the mechanical effects of blood cells or biochemical molecules, which it will take it into account in the future work to continue whit this project.

Chapter 6 Conclusions and Future Work

6.1   Conclusions

•   A methodological approach for automatic 3D geometric analysis and generation of a tetrahedral computational mesh from Synchrotron and μCT data of vascular networks from a tail and a limb of a mouse was defined. The computational mesh is intended for numerical analysis of blood flow within these vascular vessels.

•   This methodology was applied to images from Synchrotron and μCT but it can be applied in general to other volumetric data, especially where the DICOM standard is used. The methodology we set up for mesh generation allowed producing computational mesh that shows good resolution and element skewness.

•   The proposed technique is fast, accurate and reproducible, and can be a useful tool for the evaluation of micro-vascular networks fluid dynamics.

•   Results in different networks indicate the heterogeneity of fluid flow distribution within the vessels with values ranging between 0 and 3 times the inlet velocity. Respect to the vessels with a velocity equal to zero m s^{-1} means that these vessels are not well connected to the rest of the network, and the blood cannot pass through them and in this case the cells that surround these "non-functional" vessels do not receive the nutrients and oxygen from the blood necessary to survive.

•   The values of WSS obtained are within the physiological range found in the human body reported in literature. Results indicate the heterogeneity of WSS distribution within the vessels. These mechanical stimuli play an important role in angiogenesis regulating the cytoskeletal organization, as a signal transduction, in gene expression, and a wide variety of EC functions, including migration, proliferation, and ECM remodeling.

6.2 Future work

The short term future plan to continue with the development of this project involves some important task.

Task 1: The next step will be to make a comparison of in silico results with in vivo results on many different samples to determine the functionality of the angiogenic process in tissue regeneration.

Task 2: Also it is necessary to obtain data in different time points of growth to validate the methodology and to define realistic and accurate boundary conditions to ensure a proper physiological interpretation of the results. Then it will necessary to perform several analyses on different vascular networks to investigate the angiogenic functionality of the scaffolds

Task 3: Once the methodology has been assessed in different samples it will be define a validation of the model building a scale prototype of a sub-volume network, to quantify the fluid flow distribution inside the vessels to compare the obtained results, with the CFD results.

Task 4: Simulate the behavior of endothelial cells around blood vessels included in the angiogenesis process using numerical simulation, to quantify the exchange of oxygen from the vessels into the cells, in order to relate the functionality of vascular networks during angiogenesis in different scaffolds with the gas exchange necessary for the preservation of cells and tissue surrounding these vessels.

Task 5: In order to evaluate the functionality of the vascular networks development within the scaffolds design in the Angioscaff Project, it will perform CFD analysis of the resulting samples in different points of growth to quantify the volume of functional network.

	Sept-Dec 11	Janu-Sept 12	Sept-Dec 12	Janu-Sept 13	Sept-Dec 13
Task 1					
Task 2					
Task 3					
Task 4					
Task 5					

References

[1] S. Ghanaati, M.J. Webber, R.E. Unger, C. Orth, J.F. Hulvat, S.E. Kiehna, M. Barbeck, A. Rasic, S.I. Stupp, and C.J. Kirkpatrick, "Dynamic in vivo biocompatibility of angiogenic peptide amphiphile nanofibers.," *Biomaterials*, vol. 30, Oct. 2009, pp. 6202-12.

[2] M.W. Laschke, Y. Harder, M. Amon, I. Martin, J. Farhadi, A. Ring, N. Torio-Padron, R. Schramm, M. Rücker, D. Junker, J.M. Häufel, C. Carvalho, M. Heberer, G. Germann, B. Vollmar, and M.D. Menger, "Angiogenesis in tissue engineering: breathing life into constructed tissue substitutes.," *Tissue engineering*, vol. 12, Aug. 2006, pp. 2093-104.

[3] A. Hegen, A. Blois, C.E. Tiron, M. Hellesøy, D.R. Micklem, J.E. N, L.A. Akslen, and J.B. Lorens, "Efficient in vivo vascularization of tissue-engineering scaffolds," *Tissue Engineering*, 2011, pp. 52-62.

[4] G.S. Lee, N. Filipovic, L.F. Miele, M. Lin, D.C. Simpson, B. Giney, M. a Konerding, A. Tsuda, and S.J. Mentzer, "Blood flow shapes intravascular pillar geometry in the chick chorioallantoic membrane.," *Journal of angiogenesis research*, vol. 2, Jan. 2010, p. 11.

[5] R. Gödde and H. Kurz, "Structural and biophysical simulation of angiogenesis and vascular remodeling.," *Developmental dynamics : an official publication of the American Association of Anatomists*, vol. 220, Apr. 2001, pp. 387-401.

[6] S.R. McDougall, a R. a Anderson, M. a J. Chaplain, and J. a Sherratt, "Mathematical modelling of flow through vascular networks: implications for tumour-induced angiogenesis and chemotherapy strategies.," *Bulletin of mathematical biology*, vol. 64, Jul. 2002, pp. 673-702.

[7] J. Folkman, "Clinical applications of research on angiogenesis," *The New England Journal of Medicine*, vol. 333, 1995, pp. 1757-1763.

[8] T.C. Skalak and R.J. Price, "The role of mechanical stresses in microvascular remodeling.," *Microcirculation (New York, N.Y. : 1994)*, vol. 3, Jun. 1996, pp. 143-65.

[9] Y.-T. Shiu, J.A. Weiss, J.B. Hoying, M.N. Iwamoto, I.S. Joung, and C.T. Quam, "The role of mechanical stresses in angiogenesis.," *Critical reviews in biomedical engineering*, vol. 33, Jan. 2005, pp. 431-510.

[10] P. Carmeliet, "Mechanisms of angiogenesis and arteriogenesis.," *Nature medicine*, vol. 6, Apr. 2000, pp. 389-95.

[11] P. Carmeliet, "Manipulating angiogenesis in medicine.," *Journal of internal medicine*, vol. 255, May. 2004, pp. 538-61.

[12] E. Binzen, a Lendlein, S. Kelch, D. Rickert, and R.P. Franke, "Biomaterial-microvasculature interaction on polymers after implantation in mice.," *Clinical hemorheology and microcirculation*, vol. 30, Jan. 2004, pp. 283-8.

[13] D.E. Ingber, "Mechanical Signaling and the Cellular Response to Extracellular Matrix in Angiogenesis and Cardiovascular Physiology," *Circulation Research*, vol. 91, Nov. 2002, pp. 877-887.

[14] B.C. Berk, J.I. Abe, W. Min, J. Surapisitchat, and C. Yan, "Endothelial atheroprotective and anti-inflammatory mechanisms.," *Annals of the New York Academy of Sciences*, vol. 947, Dec. 2001, pp. 93-109; discussion 109-11.

[15] E. Clark, "Studies on the growth of blood vessels in the tail of the frog larvae," *Am J Anat*, 1918, pp. 37-88.

[16] B. Rather, A. Hoffman, F. Shoen, and J. Lemons, *Biomaterials Science: an introduction to materials in medicine*, 2004.

[17] K.H. Bouhadir and D.J. Mooney, "Promoting angiogenesis in engineered tissues.," *Journal of drug targeting*, vol. 9, Jan. 2001, pp. 397-406.

[18] J.J. Moon and J.L. West, "Vascularization of engineered tissues: approaches to promote angio-genesis in biomaterials.," *Current topics in medicinal chemistry*, vol. 8, Jan. 2008, pp. 300-10.

[19] P. Young, T.B.H. Beresford-West, S.R.L. Coward, B. Notarberardino, B. Walker, and A. Abdul-Aziz, "An efficient approach to converting three-dimensional image data into highly accurate computational models.," *Mathematical, physical, and engineering sciences*, vol. 366, Sep. 2008, pp. 3155-73.

[20] Center for NDE, "NDT Resorce centre."

[21] F. Peyrin, "Investigation of bone with synchrotron radiation imaging: from micro to nano.," *Osteoporosis international : a journal established as result of cooperation between the European Foundation for Osteoporosis and the National Osteoporosis Foundation of the USA*, vol. 20, Jun. 2009, pp. 1057-63.

[22] D.M.L. Cooper, B. Erickson, a G. Peele, K. Hannah, C.D.L. Thomas, and J.G. Clement, "Visualization of 3D osteon morphology by synchrotron radiation micro-CT.," *Journal of anatomy*, Jun. 2011.

[23] J.R. Cebral, M. a Castro, J.E. Burgess, R.S. Pergolizzi, M.J. Sheridan, and C.M. Putman, "Characterization of cerebral aneurysms for assessing risk of rupture by using patient-specific computational hemodynamics models.," *AJNR. American journal of neuroradiology*, vol. 26, 2005, pp. 2550-9.

[24] W.E. Lorensen and H.E. Cline, "Marching cubes: a high resolution 3D surface construction algorithm.," *Computer*, vol. 21, 1987, pp. 163-169.

[25] S. Software, "Simpleware ScanIP+FE+CAD Reference Guide v4.2."

[26] F. Labelle, *Tetrahedral Mesh Generation with Good Dihedral Angles Using Point Lattices*, California: 2007.

[27] L.-D. Jou, C.M. Quick, W.L. Young, M.T. Lawton, R. Higashida, A. Martin, and D. Saloner, "Computational approach to quantifying hemodynamic forces in giant cerebral aneurysms.," *AJNR. American journal of neuroradiology*, vol. 24, Oct. 2003, pp. 1804-10.

[28] T. Hassan, E.V. Timofeev, T. Saito, H. Shimizu, M. Ezura, T. Tominaga, A. Takahashi, and K. Takayama, "Computational replicas: anatomic reconstructions of cerebral vessels as volume numerical grids at three-dimensional angiography.," *AJNR. American journal of neuroradiology*, vol. 25, Sep. 2004, pp. 1356-65.

[29] S. Ding, J. Tu, C.P. Cheung, and F. Thien, "Geometric Model Generation for CFD Simulation of Blood and Air Flows," 2007, pp. 3-6.

[30] E.R. Raman, V.J. Vanhuyse, and M.F. Roberts, "Mathematical circulation model for the blood-flow-heat-loss relationship in the rat tail.," *Physics in medicine and biology*, vol. 32, Jul. 1987, pp. 859-75.